Validation of *AGK* knockout as a target of immune checkpoint blockade therapy for colorectal cancer.

A Thesis

submitted to

Indian Institute of Science Education and Research Pune in partial fulfilment of the requirements for the BS-MS Dual Degree Programme

by

Kanikar Shrihar Atul

Indian Institute of Science Education and Research Pune

Dr. Homi Bhabha Road,

Pashan, Pune 411008, INDIA.

Date: April, 2023

Under the guidance of

Supervisor: Prof. Dr. Florian Greten

Director, Georg-Speyer-Haus, Institute for Tumor Biology and Experimental Therapy, Frankfurt am Main, Germany.

From May 2022 to Mar 2023

INDIAN INSTITUTE OF SCIENCE EDUCATION AND RESEARCH PUNE

Certificate.

This is to certify that this dissertation entitled “Validation of *AGK* knockout as a target of immune checkpoint blockade therapy for colorectal cancer” towards the partial fulfilment of the BS-MS dual degree programme at the Indian Institute of Science Education and Research, Pune represents study/work carried out by Kanikar Shrihar Atul at the Georg-Speyer-Haus, Institute for Tumor Biology and Experimental Therapy, Frankfurt am Main, Germany, under the supervision of Prof. Dr. Florian Greten, Director, Georg-Speyer-Haus, Institute for Tumor Biology and Experimental Therapy, Frankfurt am Main, Germany, during the academic year 2022-2023.

Florian Greten

Committee:

Prof. Dr. Florian Greten Frankfurt, 19.04.2023

Prof. Dr. Satyajit Rath

I dedicate this thesis to my entire family, especially my parents and my brother for their continued support and guidance in attempting to pursue my career in academia.

Declaration.

I hereby declare that the matter embodied in the report entitled “Validation of *AGK* knockout as a target of immune checkpoint blockade therapy for colorectal cancer” are the results of the work carried out by me at the Georg-Speyer-Haus, Institute for Tumor Biology and Experimental Therapy, Frankfurt, Germany, as my MS thesis for the BS-MS program of Department of Biology, Indian Institute of Science Education and Research, Pune, under the supervision of Prof. Dr. Florian Greten and the same has not been submitted elsewhere for any other degree.

Shrihar Kanikar

Date: 28.03.23

Table of Contents.

List of tables.

List of Figures.

15	Quantification of Monoclonal clones of CMT93-Cas9-*PDL1*sgRNA line for PDL1 knockout.
16	Vector map of pMD2.G.
17	Gene interaction network of AGK with APC, TGFBR2, TP53 and KRAS.

Abstract

The evolution of tumor-immune interactions from tumor protective to tumor promoting, has been of recent interest in the field. The immune system plays a significant role in the tumor initiation, promotion/maintenance, and metastasis/growth, as observed in multiple cancers including colorectal cancer. Immunotherapies targeting checkpoint inhibitors (anti-PD1/PDL1, anti-CTLA4)show efficacious results in both patient treatments and clinical trial studies in some cancers like multiple myeloma and advanced lung cancer, but not in all. This is further complicated by tumor resistance to existing therapies and their consequent failures. Therefore there is a constant need to search for novel targets with a translational application. Colorectal cancer still remains a huge burden on the human population. With the advent of CRISPR technology and possibility to perform genome wide CRISPR screens, novel therapeutic targets can be discovered using in vivo mouse model systems with the potential to work in conjunction with anti-PD1/PDL1 and anti-CTLA4 treatment. Based on a previously performed kinome screen, this thesis attempts to validate the functional role of *AGK* knockout as a potential therapeutic target of Immune checkpoint blockade therapy for colorectal cancer, using mice derived organoids as model system.

Acknowledgements.

I sincerely thank Prof. Dr. Florian Greten and Prof. Dr. Satyajit Rath for their continued academic guidance. I thank Prof. Dr. Florian Greten for his supervision for the entire duration of the thesis. I thank the lab members especially Dr. Yasamin Dabiri and Dr. Fatih Cateci for their reliable technical assistance. I thank the lab members and others in the institute for the wonderful working experience during my stay at the Georg-Speyer-Haus, Institute for Tumor Biology and Experimental Therapy. I thank Stefanie Schütt for administrative and logistical support during the stay in Frankfurt.

Contributions.

Contributor Name	Contribution
Prof. Dr. Florian Greten	Conceptualization Ideas
Shrihar Kanikar	Methodology
—	Software
Shrihar Kanikar	Validation
Shrihar Kanikar	Formal analysis
Shrihar Kanikar	Investigation
Prof.Dr. Florian Greten	Resources
Shrihar Kanikar	Data Curation
Shrihar Kanikar	Writing - original draft preparation
Shrihar Kanikar, Prof. Dr. Florian Greten and Prof. Dr. Satyajit Rath	Writing - review and editing
—	Visualisation
Prof. Dr. Florian Greten	Supervision
—	Project administration
Prof. Dr. Florian Greten	Funding acquisition

Chapter 1: Introduction

The ability of the immune cells to recognize and infiltrate the tumor stroma was first recognized by Rudolf Virchow in the late 19th century which served as a preliminary evidence for the role played by the immune system in tumorigenesis. In the first decade of the 20th century Paul Ehrlich hypothesised the active role played by the immune system in reducing the instances of cancer, a concept today known as cancer immunosurveillance. Accumulating data since then led to the establishment of Cancer immunology as a field.Today we know that cancer immunosurveillance is part of a much more broader concept known as cancer immunoediting which underscores the dual role played by the immune system in tumorigenesis.

Even under homeostatic conditions, DNA is often directly or indirectly subject to damage and unwanted mutations through multiple sources like carcinogens, UV, chronic inflammation, viral infections, etc which can potentially lead to malignant transformations. As a means to defend against the aforementioned, various intracellular and intercellular mechanisms are in place, where the former acts as a first line of defence wherein the damaged cells/tissues undergo apoptosis (if unable to repair). If this fails and leads to a malignant transformation, the neo-antigens (along with others like NKG2D ligands, etc) expressed by the transformed cells, are detected by the immune cells and these cells are then eliminated by the immune system (cancer immunosurveillance). Sometimes, during this process, few cancer cells acquire mutations enabling them to resist the negative immune pressure. As a result these cells are selected and continue to expand. This gives rise to a situation, where both the immune system and cancer cells are continuously adapting and evolving in time in an antagonistic fashion ultimately giving rise to an equilibrium state termed cancer persistence or dormancy wherein the immune system is continuously clearing cancer cells and cancer cells are continuously evolving to resist the immune system. During successful tumorigenesis, cancer cells escape the immune system leading to a full blown cancer, which involves remodelling of the tumor microenvironment from “anti-tumor” to “pro-tumor”. This is the concept of

Cancer immunoediting which can be said to occur in three phases: Phase 1: Elimination, Phase 2: Equilibrium, Phase 3: Escape. Each of these phases can be characterised by involvement of key molecular and cellular players.

The third most common cancer in the world is colorectal cancer (CRC). Even in high-income nations, the incidence, prevalence, and death of CRC remain high despite some advancements in screening and treatment. Due to the inefficiency of current treatment plans, which include chemotherapy and/or targeted therapy, optionally paired with radiation therapy for late-stage and advanced metastatic illness, patients diagnosed with stage 4 CRC have a survival probability at 5 years of less than 10%.(Miller *et al.*, 2019) This emphasises the urgent need to understand the pathogenesis of colorectal cancers on molecular level. Currently, based on the molecular and genetic signatures, CRC is classified into majorly 4 subtypes, CMS1, CMS2, CMS3, and CMS4, each with a distinct feature (Guinney *et al.*, 2015).

Figure 1: CMS classification and associated pathways in CRC development (Schmitt and Greten, 2021).

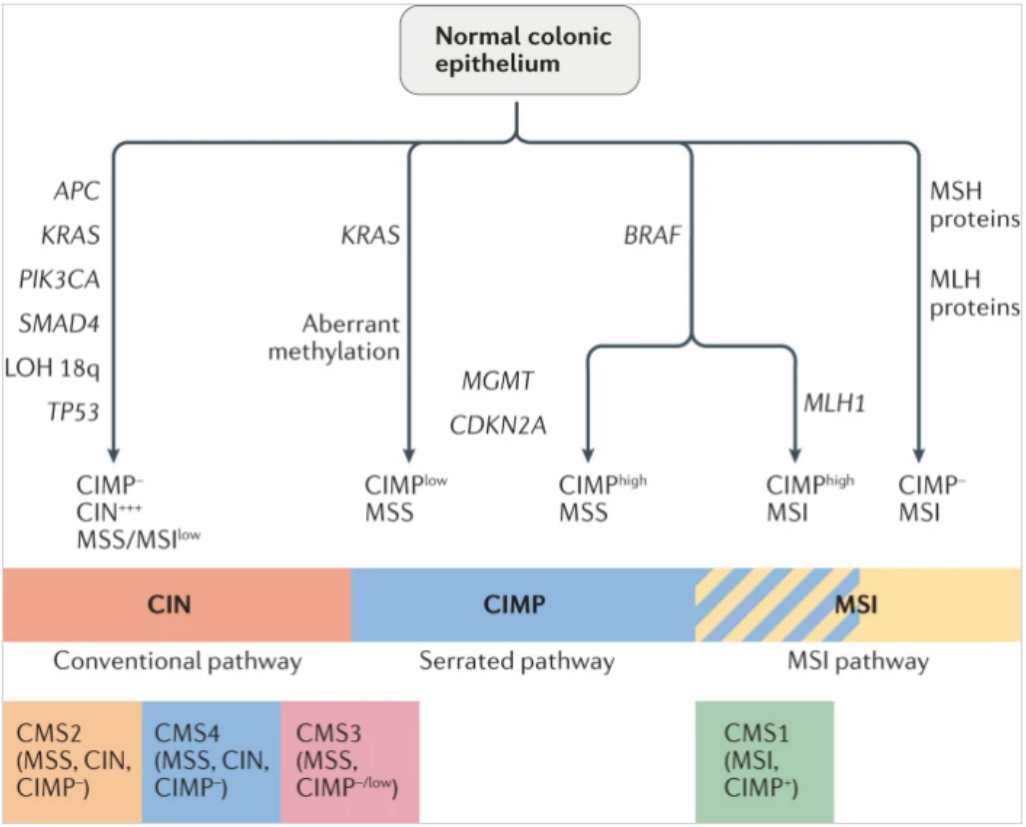

Description: Analysis of large CRC datasets revealed that majority of the CRC cases are caused by the conventional Chromosome instability pathway, initiated by mutation in *APC* which is loss of heterozygosity of chromosome 18 (LOH 18q), followed by mutations in *KRAS*, *PIK3CA*, *SMAD4* and *TP53* mutation. Significant levels of chromosome instability (CIN+++), microsatellite stability (MSS), and, no or very little levels of the CpG island methylation (CIMP–) are linked to CRC development via this route.The serrated pathway, which can be further classified into BRAF-mutant CIMPhigh MSS tumours, KRAS-mutant CIMPlow Microsatellite stable tumours, and BRAF mutant CIMPhigh MSI tumours, accounts for about 20–30% of instances of CRC. Serrated tumours usually have MGMT, CDKN2A, or MLH1 gene silencing. The MSI route, which is a third pathway of CRC formation , is brought on by failure of DNA mismatch repair genes, for instance the ones which produce MLH proteins or MSH proteins.(Schmitt and Greten, 2021),(Shen *et al.*, 2007)

Cancer progression is accompanied by extensive remodelling of the tumor microenvironment (TME) which is often associated with a tumor promoting phenotype. The TME also plays a huge role in treatment resistance and clonal evolution of cancer (Baghban *et al.*, 2020) . The efficacies of many of the contemporary treatments for cancer including immunotherapies are heavily dependent on the state of the TME. In the context of CRC, Tumor Microenvironment is mainly composed of the Microbiota, extra-cellular matrix, immune cells, vascular cells, soluble factors and molecular mediators, all of which contribute to tumor immunomodulation. It mainly occurs in 4 different ways (Plundrich *et al.*, 2022).

A] Cell-cell receptors interactions. B] Interactions with Soluble factors. C] Cell-ECM interactions. D] Interactions with the Microbiome.

Figure 2: Immunomodulation in CRC Tumor microenvironment (Plundrich *et al.*, 2022)

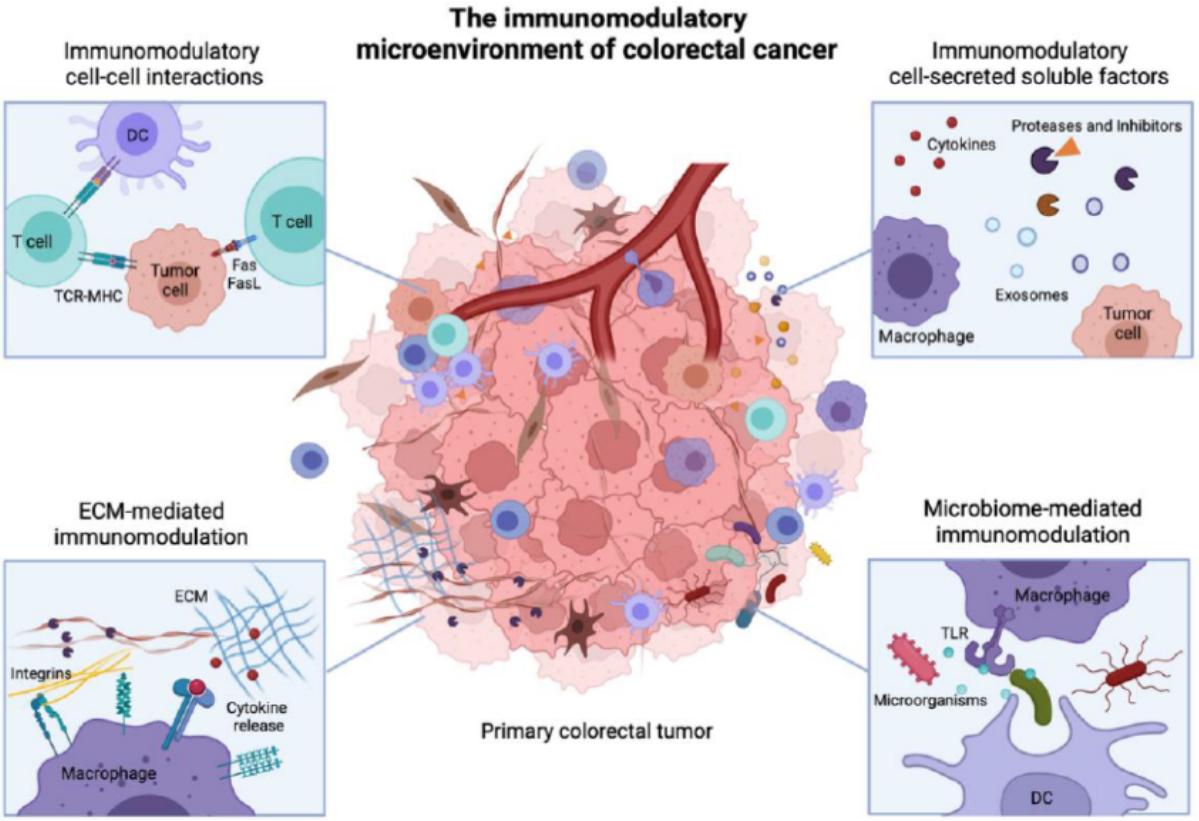

Description: Overview of the 4 main ways in which CRC immune microenvironment is modulated. ECM: Extracellular matrix, DC: Dentritc cells.

In context of the net effect on the immune system, all of these interactions can be argued to converge at the inherent “offensive”, that is cytotoxic arm, and “defensive” that is cytoprotective arm, of the immune system and the net effect, either immune activation (anti-tumor) or immune suppression (Pro-tumor) depends on the cumulative effect of these myriad interactions. As is the case with majority of cancers, immune evasion and pro-tumor microenvironment remodelling occurs, primarily by exploiting the inherent feedback mechanisms of the immune system physiology wherein immune-activating pathways are inhibited and immune-inhibiting pathways employing PDL1/2, CTLA4 are hyperactivated in the TME by the tumor cells. (Plundrich *et al.*, 2022)

This phenomenon across cancers prompted the need to investigate the effects on immunosuppression by usage of inhibitors (like anti-PDL1 antibodies) of various immune-inhibitory ligands, and to validate clearance of the tumor cells by the immune system. These inhibitors are essentially targeting the checkpoint proteins of the immune system physiology and therefore this line of treatment is termed as Immune checkpoint blockade therapy, which is a subset of a broader concept called immunotherapy. Immunotherapy relies on harnessing the existing abilities of the immune system to clear tumor cells. (Ribas and Wolchok, 2018)

Concept of immunoscore: Representation in terms of CD8+ T cells. .

It can be argued that within the CRC TME, on the level of T cell phenotypic behaviour, there are three possible outcomes. First, No activation/priming of T cells against tumor. Second, Exhaustion of tumor specific CD8+ T cells due to insufficient activation, etc. Third, Sufficient tumor specific CD8+ T cell activation but rendered non functional due to local immunosuppressive environment. Therefore all the CRC tumor classes in the context of immune states fall into one of these three categories. Compared to the classical TNM (Tumor-Node-Metastasis) system of tumor classification, a new concept for patient stratification based on the type, density and location of immune cells in the tumor niche, showed more accuracy.(Mlecnik *et al.*, 2011) This idea lead to the development of the concept of immunoscore, which now is heavily implemented (Galluzzi *et al.*, 2012) (Galon *et al.*, 2006) (Galon *et al.*, 2013) (Angell and Galon, 2013) (Galon *et al.*, 2007). It is based on the quantification of the CD3 and CD8 lymphocyte population both at the tumor centre and the invasive margin (Galon *et al.*, 2013) (Pagès *et al.*, 2009). The immunoscore ranges from 0 (I0) to 4 (I4) wherein I0 and I4 denote low and high densities of both cell types (CD3 and CD8) in both locations (tumor centre and invasive margins) respectively. Therefore tumors with high infiltration or high immunoscore (I4) are called “Hot” whereas tumor with low infiltration or low immunoscore (I0) are called “Cold” tumors (Galon and Bruni, 2019). Therefore the overall goal for an efficient immunotherapeutic treatment would be conversion of “Cold” tumor into a “Hot” tumor for successful tumor clearance.

Despite the strong theoretical foundation of immunotherapy, it has not shown promising results in treatment of the majority of colorectal cancer cases. For instance CRC tumors with high DNA mismatch repair deficiency and/or microsatellite instability show partial success, with increased T cell infiltration post Immune checkpoint blockade therapy but the treatment fails for CRC tumors with microsatellite stability and proficient DNA mismatch repair, which represents the majority of CRC cases (André *et al.*, 2020) (Ganesh *et al.*, 2019) . Therefore there is a constant need to search for novel targets that work in conjunction (or independently) with contemporary immune checkpoint blockade therapy. Given the myriad of potential pathways exploited by tumor cells for immune evasion, finding a key node that renders the tumor susceptible to anti-tumor immune activity, and ultimately clearance, is an enigma. However with the advent of CRISPR (M *et al.*, 2012) and robust next generation sequencing technologies (Guan *et al.*, 2012), it is now possible to perform large scale loss of function CRISPR screens using lentiviral vectors in appropriate model systems to screen for novel targets. Literature reports various genome wide loss of function CRISPR screens performed across cancers and alludes to role played by certain key players in promoting tumorigenesis and that their knockout can be a possible therapeutic intervention (Makhov *et al.*, 2020) (Dai *et al.*, 2021). Kinases are heavily implicated in cancer biology and the dysregulation of their associated pathways often promotes immune evasion for cancer cells. For instance the GAS9/AXL pathway (AXL is a receptor tyrosine kinase) promotes immunosuppressive TME and causes immune evasion (Son and Jeong, 2021). Tyrosine Kinases also play a significant role in growth and proliferation and hence their targeting in cancer has been an attractive therapeutic intervention (Traxler, 2003).

Given this motivation and resources, the host laboratory of Prof. Dr. Florian Greten performed a loss of function CRISPR screen with a pooled library screening approach in a mouse cell line CT26.WT. The brie kinome library containing 2,852 unique guides targeting 713 mouse kinase genes, with 4 guides per Kinase, along with 100 non specific control guides was used (Doench *et al.*, 2016). The library was obtained in a two vector system in lentiguide-Puro backbone (Sanjana *et al.*, 2014). Thus the Cas9 was expressed in a different vector namely pCW-Cas9-Blast, which is doxycycline-inducible, Cas9 expressing vector with Blasticidin resistance. Post

generation of lentiviruses from these vectors, the cell line was infected with a low MOI and the stably transduced polyclonal population of CT26.WT cells was transplanted subcutaneously in mice. Mice were kept on doxycycline to induce Cas9 expression and to allow gene editing. Changes in Immune cell infiltration and physical parameters like size of the tumor, was used as a readout and tumor samples were sequenced to screen for appropriate targets causing increased immune cell infiltration. This screen generated *AGK* as a promising hit. Figure 3 shows the experimental strategy employed for the screen.

Figure 3: Experimental strategy for *in vivo* loss of function CRISPR screen.

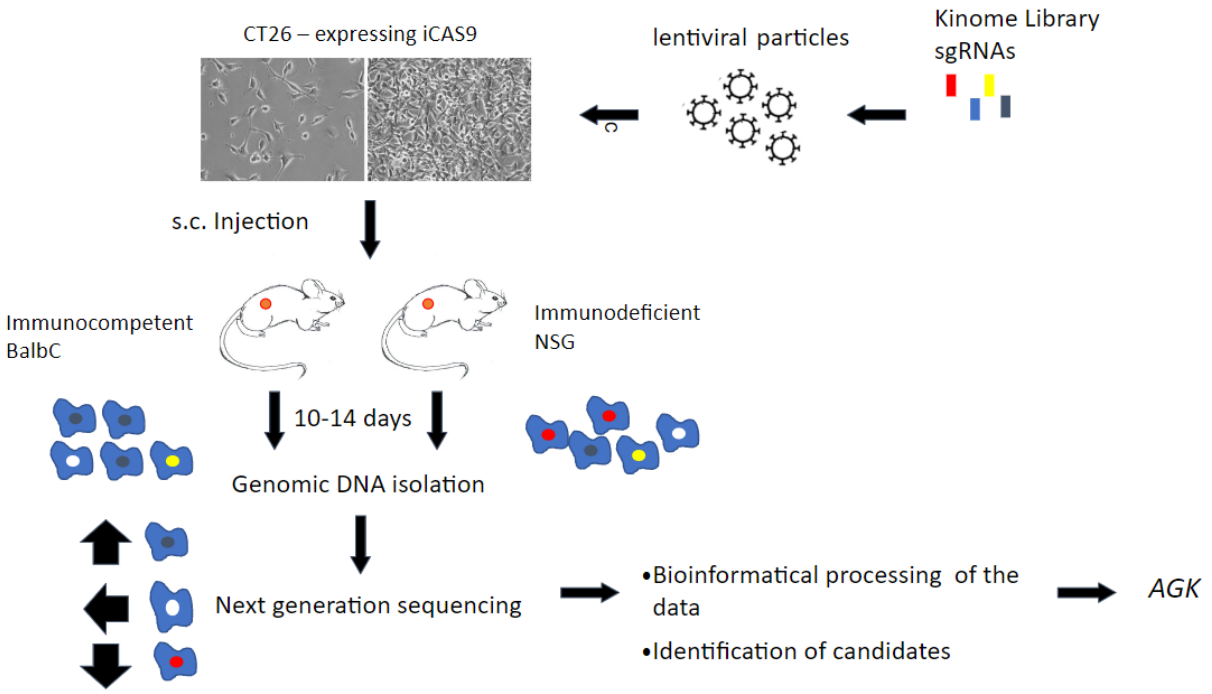

Description: CT26.WT cell line stably expressing iCas9 from pCW_Cas9 doxycycline inducible vector, was transduced with brie Kinome library at a low MOI and selected polyclonal population was transplanted subcutaneously in immuno-competant and immuno-deficient mice. Genomic DNA from the tumors was isolated and sequenced to screen for sgRNAs enriched or depleted as compared to genomic data from

immunodeficient mice. This lead to identification of *AGK* as a potential target whose knockout causes increased immune infiltration and anti-tumor activity.

Despite the initial success of the screen, there were two major drawbacks. First, Post subcutaneous transplantation of stably transduced polyclonal CT26.WT cell line in mice, in vivo expression of foreign proteins like Cas9, antibiotic resistance proteins,etc lead to induced immunogenicity causing no significant difference between experimental and control groups in terms of immune cell infiltration and tumor size. Second, CT26.WT cell line seemed to be growing very aggressively *in vivo* and therefore the genome editing may not have been very efficient. Thus in order to successfully validate *AGK* as a potential therapeutic target, it was imperative to get rid of these aforementioned problems. This problem of induced in vivo immunogenicity against foreign proteins like Cas9, etc , in concordance with the data in the lab, was proven in the literature (Dubrot *et al.*, 2021). In order to get rid of this problem Dubrot et al generated new lentiviral vectors which allowed selective removal of antigens like Cas9, fluorescent reporter genes,antibiotic resistance genes and others, post sufficient genome editing in vitro. Only the sgRNA insert remains in the genome which serves as a barcode for sequencing. This was achieved by using the Cre-Lox system. The two SCAR vectors contain Lox P sites flanking the regions which are intended to be removed post genome editing. To transiently express Cre in the cells, integrase deficient lentiviruses are used which carry a point mutation in the integrase gene of the psPAX2 vector. This strategy served as a remarkable solution to avoid the aforementioned problems however with a small drawback, which is, the genome editing does not occur in vivo. The edited population is transplanted in vivo. So if this method was to be applied to the loss of function CRISPR screen then it would be an indirect in vivo screen. Figure 4 shows the experimental approach while utilising the selective CRISPR antigen removal (SCAR) lentiviral vector system (Dubrot *et al.*, 2021).

Figure 4: Genome editing strategy using the SCAR vector.

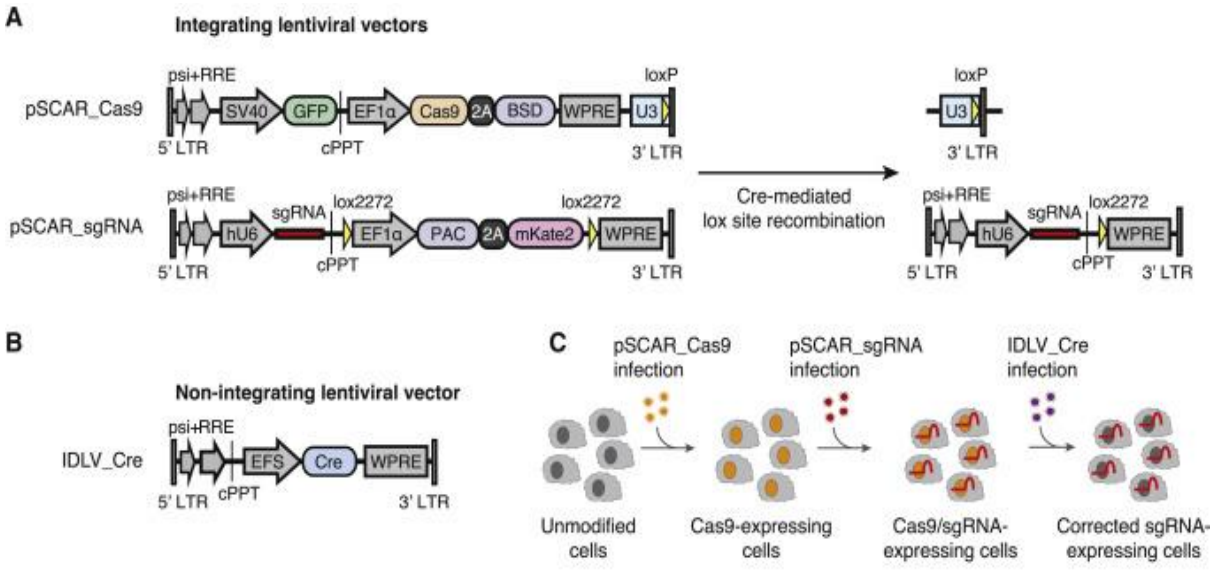

Description: A: Design for pSCAR_Cas9 and pSCAR_sgRNA lentiviral constructs before (left) and after (right) Cre-mediated recombination. B: Design of non integrating Cre expressing lentiviral vector. C: Experimental protocol for generation of stably transduced cells that undergo Cre-mediated recombination post genome-editing. The SCAR lentiviral vectors are used sequentially to transduce cells which are then selected with appropriate antibiotics. These double positive cells are then infected with an integrase deficient lentivirus (psPAX2 mutant for integrase gene) containing the Cre vector that allows transient expression of Cre. This results in a genome edited cell population post Cre mediated recombination of the aforementioned genes. Post monitoring loss of Cas 9 and fluorescent reporters, whilst ensuring gene knockout, this population can be transplanted in vivo. The loxP sites in the two SCAR vectors are heterologous to avoid recombination between vectors. The lox P site in the SCAR_Cas9 vector duplicates post integration in the genome facilitating complete cre mediated recombination of the vector.

In order to successfully validate *AGK*'s therapeutic potential, it was imperative to avoid expression of foreign proteins that hinder the system on molecular level. Thus one possible solution was to validate *AGK* in the SCAR vector. *AGK* as known as Acyl-glycerol Kinase or Multi-substrate lipid kinases (MULK) is a recently discovered mitochondrial Lipid Kinase. It was initially discovered as one of the key mutated genes in Sangers Syndrome(Mayr *et al.*, 2012). *AGK* has both kinase dependent and kinase independent functions and is heavily implicated across multiple cancers, thrombopoiesis, metabolism, CD8 T cell function, etc. AGK is responsible for the production of LPA (Lysophosphatidic acid) and PA (Phosphatidic acid) via phosphorylation of MAG (Monoacyl glycerol) and DAG (Diacyl glycerol) (Bektas *et al.*, 2005). AGK mediates its pro-tumor functions via excess production of LPA, which is thought to play a role in cell growth and differentiation(Geraldo *et al.*, 2021). AGK is a subunit of the human TIM22 complex, which is a mitochondrial translocase that is indispensable for the translocation and assembly of mitochondrial proteins. Presence and/or activity of AGK is imperative for stabilisation of TIM22 complex. Thus AGK plays a huge role in mitochondrial physiology and membrane integrity via both kinase dependent and independent functions (Chu *et al.*, 2021) (Qiao *et al.*, 2018) (Kang *et al.*, 2017). However the role of AGK varies across cell types. For instance, AGK promotes a shift towards a more glycolytic metabolism which is essential for CD8 T cell cell function and therefore anti-tumor activity, whilst its upregulation in tumor cells promotes tumorigenesis (Hu *et al.*, 2019) (Varanasi *et al.*, 2020). AGK is one of the most commonly mutated genes across cancers and contributes to cell proliferation, drug resistance, and metastasis via key dysregulated signal transduction pathways, namely the hippo pathway, JAK-STAT3, NF-κB, PI3K-AKT, etc. It also interacts with EGF and FOXO transcription factors. Details of each of these pathway interactions with AGK are nicely reviewed by Chu et. al in their review (Chu *et al.*, 2021). Little is however known about the mechanistic action of AGK. Its function depends on the cell type and its sub-cellular localization and inhibition of AGK in cancer cells seems to be a promising therapeutic intervention. Thus with this theoretical background we sought to validate "AGK knock out in tumor cells" as a possible therapeutic intervention in conjunction (or independently) with ICB therapies in colorectal cancer.

Induced pluripotent stem cells, adult stem cells, and embryonic stem cells can all be used to create organoids, which are three-dimensional culture systems. They have the capacity for cell division, proliferation, and self-renewal. Organoids self-assemble to mimic the morphological and structural traits of the appropriate organs when stimulated by signal and/or growth factors. They offer an exceptional setting for exploring how organs develop and simulating disease processes (Yang *et al.*, 2022). In order to mimic and generate good in vitro model systems representing CMS subtypes of CRC, Varga. J. et. al generated organoids with specific mutations that enhanced tumorigenesis in AOM (Azoxymethane) model of colon cancer and ultimately represent the CMS2-4 spectrum of colon cancer. AOM is a carcinogen that causes mutations in oncogenes and tumor-suppressor genes via DNA alkylation. However, organoids derived from AOM challenged mice do contain unknown mutations and to generate organoids with known mutational background (as seen generally in CRC patients) APTK and APTKA organoids were generated. The first colon organoids were created using unchallenged Trp53fl/flTgfbr2fl/fl mice. Then, using CRISPR/Cas9, Apc deletion was introduced, and organoids were selected by removing R-spondin from the growth media (A organoids). " A" organoids were transduced with a plasmid encoding Cre recombinase to induce Trp53 and Tgfbr2 deletion, and organoids with Trp53 and Tgfbr2 deletion were selected using the MDM2 inhibitor nutlin3 (APT organoids). Subsequently, oncogenic murine KrasG12D mutation was introduced into APT organoids by retroviral infection, and puromycin was used to select the organoids that were correctly targeted (APTK organoids). Eventually, persistently infected organoids were chosen using hygromycin after constitutive AKT activation was established by the insertion of a retroviral vector expressing human myristoylated AKT (APTKA organoids) (Varga *et al.*, 2020).

Aims and objectives.

1. Overcome drawback of *in vivo* induced Immunogenicity of the initial screen.

    - Temporal analysis of Cas9 expression and downstream genome editing efficiency in APTK organoid lines stably expressing Doxycycline inducible Cas9, for transplantation of aforementioned genome edited organoid lines in mice that are NOT on doxycycline treatment.

    - Employ Usage of SCAR Vector: Generate stably transduced CMT-93 cell lines for validation of SCAR vector system, that stably express Cas 9 and *PDL1*sgRNA constructs in the SCAR vector.

    - Infect the PDL1 knocked out population with IDLV-Cre and transplant subcutaneously in mice.

    - Perform limiting dilutions

    - Generate integrase deficient lentiviruses expressing Cre for selective removal of Cas9 and antibiotic resistance genes post transduction *in vitro* and for subsequent subcutaneous transplantation in mice.

2. Improve transfection and transduction efficiencies for SCAR vectors.

    - Compare transfection efficiencies of different reagents with SCAR Cas9 vector (13.3 Kb).

    - Employ different concentration techniques for lentiviral titres.

3. Generate stably transduced APTK organoid lines for validation of *AGK*.

    - Clone *AGK* sgRNA oligos in SCAR-sgRNA-Hygro vector.
    - Generate lentiviruses harbouring appropriate SCAR vectors.
    - Perform serial transductions to generate APTK-SCAR_Cas9-SCAR *AGK*sgRNA lines.
    - Perform limiting dilutions of the lines for subsequent infection *in vitro* with integrase deficient lentiviruses expressing Cre.

Therefore, this thesis includes the attempts to elucidate the functional implications of *AGK* knockout in the context of immune checkpoint blockade therapy for colorectal cancer using APTK organoids and mice as model systems. The goal was to generate stable APTK-*AGK*sgRNA-Cas9 expressing organoid lines using lentiviral transductions, which would then be transplanted subcutaneously in mice post which the effect of knockout , of anti-PDL1 treatment would be examined. We tried to employ two different strategies to avoid the induced *in vivo* immunogenicity. First, to transplant transduced organoids (with Dox-inducible Cas9 expression) post induction *in vitro* so as to avoid Cas9 expression *in vivo.* Second, Transplant organoids transduced with SCAR vector post genome editing *in vitro* and Cre-mediated selective removal of antigens. We attempted to validate the efficacy of the SCAR vector using the CMT-93 cell line. However due to technical difficulties we could not reach the transplantation stage and therefore the in vivo validation of *AGK* knockout or the SCAR vector is beyond the scope of this thesis.

Chapter 2: Materials and Methods.

Table 1: Resource table.

Resource/Reagent	Source	Identifier/Catalogue number
Cell lines and Organoids		
CMT93	ATCC	CCL-223™
HEK 293T	ATCC	CRL-11268™
APTK	In house	NA
Bacterial strain		
NEB® Stable Competent E. coli (High Efficiency)	New England Biolabs	C3040I
Antibody		
Cas9 (7A9-3A3) mouse mAB (Alexa 647)	Cell signalling	#48796S
Plasmids/Recombinant DNA.		
pMD2.G	Addgene	#12259
psPAX2	Addgene	#12260

psPAX2-D64V (IDLV)	Addgene	#63586
SCAR-Cas9-Blast	Addgene	#162074
SCAR-sgRNA-hygro	Addgene	#162070
IDLV-Cre	Addgene	#162073
pcW-Cas9	Addgene	#83481
pUC19 Vector	New England biolabs	C3040I
Chemicals and restriction enzymes		
Lipofectamine 2000 Transfection reagent	Thermofisher Scientific	11668027
Lipofectamine 3000 Transfection reagent	Thermofisher Scientific	L3000015
Lipofectamine Ltx Transfection reagent	Thermofisher Scientific	15338030
Polyjet Transfection reagent	Signa Gen Laboratories	SL 100688-5
Calcium chloride	In house	NA
HBS buffer solution	In house	NA
DMEM	ThermoFisher Scientific	11965092
Glutamax	ThermoFisher Scientific	#35050061

HEPES	ThermoFisher Scientific	#15630080
Adv. DMEM F12	ThermoFisher Scientific	#12634010
Opti-Mem	ThermoFisher Scientific	31985070
Puromycin dihydrochloride	Merck	#58-58-2
Doxycycline hyclate	Sigma aldrich	D9891-10G
Hygromycin B	ThermoFisher Scientific	#10687010
Ampicillin	In house	NA
Blasticidin S -hydrochloride	Sigma-Aldrich	# 15205
Penicillin/ Streptomycin	ThermoFisher Scientific	# 15070063
Accutase cell dissociation reagent	ThermoFisher Scientific	# A1110501
B-27 supplement	ThermoFisher Scientific	# 12587010
N-2 supplement	ThermoFisher Scientific	# 17502048
N-Acetylcysteine	Sigma-Aldrich	# A9165
BME Type II	R&D Systems	#3533-005-02P
Matrigel	Corning	# 356231
Cell recovery solution	Corning	CLS354253

0.05% Trypsin EDTA	ThermoFisher Scientific	# 25300054
0.25% Trypsin EDTA	ThermoFisher Scientific	#25200056
SuperScriptII Reverse Transcriptase	Invitrogen	# 18064-014
SYBR Green Master Mix	Roche	# 04913914001
OligoDT	Invitrogen	# N8080128
DNTP	Invitrogen	# AM8200
T4 ligation buffer, 10×	New England Biolabs	M0202S
T4 PNK	New England Biolabs	M0201S
Stick together DNA ligase buffer 2×	New England Biolabs	B0535S
T7 ligase	New England Biolabs	M0318S
BsmB1.	New England Biolabs	R0739S
NotI	New England Biolabs	R3189S
SacI	New England Biolabs	R3156S
AgeI	New England Biolabs	R3552S

SapI	New England Biolabs	R0569S
3M Sodium acetate	In house	NA
Ribonuclease inhibitor RNAseOUT™	Invitrogen	# 10777019
NEB® 10-beta/Stable Outgrowth Medium	New England Biolabs	C3040I
Commercial Kits and products		
Qiagen DNA mini kit	Qiagen	12123
Qiagen DNA maxi kit	Qiagen	12162
Qiagen RNeasy mini kit	Qiagen	74004
Vivaspin 6, 10kDa, MWCO Polyethersulfone	Merck	GE28-9322-96
Oligos and primers		
PDL1_sgRNA#1 fw	Eurofins Genomics	TGCTGCATAATCAGCTACGG
PDL1_sgRNA#2 fw	Eurofins Genomics	TCCAAAGGACTTGTACGTGG
PDL1_sgRNA#3 fw	Eurofins Genomics	CTCAGCACAGCAACTTCAGG
PDL1_sgRNA#4 fw		GCTTGCGTTAGTGGTGTACT

AGK_sgRNA#1 fw		ATATTGCAGACGGATTATGA
AGK_sgRNA#2 fw		CTCTGAAAGATCCCCACCGG
AGK_sgRNA#3 fw		GAAATACCCTTTGCAAGCTG
AGK_sgRNA#4 fw		AGTACTGAGAAGAACAGATG
NMT_sgRNA#9 fw		AAGCCTACTTCACCGGTCGG
Softwares		
GraphPad Prism 9	GraphPad	NA
TaqMan® Genotyper™ Software	ThermoFisher Scientific	NA
ImageJ Software	Open Source	NA
Cytoscape (GeneMANIA)	Open Source	NA

Method details.

Cloning of sgRNA oligos in SCAR vector.

Oligo Annealing: Four sgRNA oligos each for *PDL1* and *AGK* (mentioned above in resource table) were cloned in the SCAR_sgRNA-hygro vector following the protocol as described by Ran et. al. with certain modifications(Ran *et al.*, 2013). Sequences for the aforementioned oligos were taken from the brie kinome library and oligos were commercially ordered. Forward strand of each oligo was appended with the

sequence “CACCG” and the reverse strand was appended with “AAAC” on the 5 prime end of each strand. These are the restriction sites for BsmB1 restriction enzyme which was used for the cloning reaction. Oligo complementary annealing was performed in a total of 10ul reaction volume wherein 1ul each of forward oligo strand, reverse oligo strand, T4 ligation buffer 10X, T4 PNK was added and the total volume was made up with 6ul of nuclease free water. Phosphorylated oligos were allowed to anneal and the annealing reaction was performed in the qPCR thermocycler machine by using the following parameters: 37 °C for 30 min; 95 °C for 5 min; ramp down to 25 °C at 5 °C min^{-1}.

Cloning: The annealed oligos were diluted 1:10 with nuclease free water and 1ul of this was used for the cloning reaction. The cloning reaction (total volume 20ul) consisted of the following reaction mixture.

Table 2: Cloning reaction mix.

Reagent	Volume
Annealed oligos (1:10)	1µl
SCAR vector (~600 ng/ul).	1µl
Stick together DNA ligation buffer, 2×	10µl
T7 DNA ligase	1µl
BSA	1µl
BsmB1	1µl
Nuclease free water	Up to total volume of 20µl

The cloning reaction was allowed to happen in the PCR machine with the following settings: 100 cycles where one cycle was 37°C for 5 mins and 20°C for 5 mins.

Transformation: The resulting cloned sgRNA oligos in SCAR-sgRNA-hygro vector was transformed in NEB® Stable Competent *E. coli* (High Efficiency). The transformation was done with a heat shock of 42°C for 30 seconds. The transformed bacteria were allowed to grow in NEB® 10-beta/Stable Outgrowth Medium for 1 hour at 30°C at 300 rpm before plating on LB-agar + Amp plates (Selection with ampicillin). The plates were incubated overnight at 30 degrees.

Validation of Cloning: Single colony from each of the transformed NEB strains with appropriate vectors was picked up and cultured in 250 ml LB+Amp (100ug/ml) medium overnight at 175 rpm and 30°C. The following day the samples were maxi and mini prepped using the Qiagen DNA maxi kit and Qiagen DNA mini kit according to the manufacturer's protocol respectively. The miniprep samples were sequenced and the cloning results were validated.

Generation of Lentivirus:

HEK 293 T cells with Passage number less than 12 were used to produce lentiviruses using the 2nd generation lentiviral system consisting of two packaging plasmids, pMD2.G and psPAX2 plasmids were used. pMD2.G plasmid encodes for the VSV-G gene and is responsible for production of envelope protein, Env. A single plasmid psPAX2 encodes for *Gag, Pol, Rev,* and *Tat* genes which are responsible for production of reverse transcriptase, integrase and other viral proteins responsible for generation of lentivirus and integration of transfer plasmid, which was the SCAR or pcWCas9 vector in our case.

HEK 293 T cells were transfected with the appropriate transfer vectors, pMD2.G, and psPAX2 at the ratio of ~ 3:1:3 respectively, using mainly three different transfection reagents, Lipofectamine, polyjet and Calcium chloride in HBS buffer. For production of integrase deficient lentivirus carrying Cre expressing transfer vector, psPAX2D64V was used instead of psPAX2. Successful transfection was confirmed with GFP fluorescence in HEK cells. For transfections, the manufacturer's protocol for each of the transfection reagents was followed. For harvesting lentivirus, media was replaced with medium of line (cell or organoid) to be infected ~20 hours post

transfection and supernatant containing lentivirus was collected at 48 and 72 hours post transfection filtered through 25µm filter, and pooled. Lentivirus was concentrated using two methods: overnight centrifugation at 10,000g, or using Vivaspin 6, 10kDa, MWCO Polyethersulfone columns. For concentration of lentivirus using Vivaspin columns, the viral supernatant was centrifuged at 1000g for 25-30 mins until the volume was reduced to 1 ml(Pirona *et al.*, 2020).

Generation of stably transduced CMT93 cell line.

CMT93 cell line was first transduced with SCAR-Cas9-Blast harbouring lentivirus. 25000 cells (Counted with haemocytometer) were infected using spinoculation method in a 96 well U bottom microtiter plate at a final volume of 200 µl containing polybrene at a concentration of 10 µg/ml. Cells were centrifuged for 3 mins at 500g and 4°C for pelleting and incubated with viral supernatant for 7-9 hours at 37°C, 5% CO_2, after which they were transferred to 6 well plates and were replaced with fresh medium. Selection of transduced cells was started 48 hrs post transduction with blasticidin at a final concentration of 10 µg/ml (Pirona *et al.*, 2020). Successful transductions were confirmed with blasticidin selection and GFP fluorescence and quantified with qPCR. This line was then subjected to limiting dilution as the goal was to generate a monoclonal cell line. Standard protocol of limiting dilution from addgene was followed to generate monoclonal CMT93-SCAR_Cas9 line. This monoclonal population was then transduced with 4 different SCAR_PDL1sgRNA-Hygro harbouring lentiviruses to generate CMT93-SCAR_Cas9-SCAR-PDL1sgRNA line using the aforementioned protocol. Double positive cells were selected using hygromycin (500 µg/ml) and blasticidin (10 µg/ml). The SCAR-sgRNA-Hygro vector contained a BFP tag, therefore the selected double positive cells were checked for both GFP and BFP. Imaging was performed on CQ1 confocal microscope.This population was then subjected to limiting dilution. All the cell lines were kept in appropriate antibiotics even after selection to avoid growth of non resistant organoids.

Generation of stably transduced APTK organoid lines.

APTK organoids were treated with cell recovery solution to remove BME followed by treatment with accutase for 10 minutes to cellularize the organoids. Single cell organoids were then infected with SCAR_Cas9-blast harbouring lentiviruses with spinoculation method which includes centrifugation at 600g at 32°C for 1 hour followed by incubation for 6 hours with the viral medium at 37°C, 5% CO_2 before resuspending in BME type 2. Polybrene at a final concentration of 5ug/ml was used. Selection was started 48 hrs post transduction for 15 days. These organoids were then transduced with SCAR-sgRNA-hygro harbouring lentiviruses, with the aforementioned protocol to generate the APTK-SCAR_cas9-SCAR_*AGK*sgRNA line. Double positive cells were selected using hygromycin (500 µg/ml) and blasticidin (10 µg/ml). Selected double positive organoids were checked for both GFP and BFP. Imaging was performed on CQ1 confocal microscope. All the organoids were kept in appropriate antibiotics even after selection to avoid growth of non resistant organoids.

Gel electrophoresis and ethanol precipitation.

Plasmid vectors were tested for recombination post maxi preps by employing gel electrophoresis and running the samples on agar gel at 120mV for ~ 1 hour. The samples were loaded post restriction digestion with appropriate enzymes for 1 hour at 37°C and stained with EtBr for imaging.
Low concentrations of DNA maxi preps were subjected to ethanol precipitation. 0.1 Volumes of 3M sodium acetate was added with 3 volumes of 100% ethanol to the DNA sample and vortexed. DNA was allowed to precipitate for 1 hour at -20°C and centrifuged at 13000 rpm at 4°C for 30 minutes. DNA pellet was washed twice with 75% ethanol at 4°C for 10 mins per wash. Pellet was air dried and suspended in appropriate volume of Endonuclease free TE buffer.

RNA isolation and RT-qPCR.

For cell lines: Cells were harvested by trypsinization by using Trypsin EDTA (0.25%)

and pelleted by centrifugation at 1200 rpm for 5 minutes and washed with cold PBS. For Organoids: Organoids were collected in cell recovery solution diluted in cold PBS. Post mechanical disruption, organoids were pelleted by centrifugation at 900 rpm for 5 minutes and washed with cold PBS. Cell and organoid pellets were lysed in 1% ß-Mercaptoethanol and vortexed for 2 minutes for homogenization. RNA isolation was performed using the Qiagen RNeasy Kit following the manufacturer's protocol. RNA quantity and quality was determined using the Nanodrop Spectrophotometer. For quantitative PCR, cDNA was synthesised from 2000 ng RNA, using Superscript II reverse transcriptase (Invitrogen). RNA was incubated with oligoDT and DNTP Mix (1 µl each) for 5 min at 65°C in a total reaction volume of 13 µl. The samples were allowed to cool down for 5 minutes on ice, and to each 4 µl of 5x First strand buffer, 1 µl DTT, 1 µl RNAseOUT™ and 1 µl Superscript II reverse transcriptase were added. Samples were incubated for 1 hour at 42°C. Synthesised cDNA was 1:10 diluted in nuclease free water before being processed into gene expression analysis with the 96 wells StepOne real time PCR Machine (Applied biosystems) using 2X FastStart Universal SYBR Green Master Mix (Roche). Livak's methods or the delta delta Ct method was used to compare gene expression values of the samples.

Quantification of Cas9 with prolonged exposure of Doxycycline in APTK-pCWCas9 with FACS.

APTK-pcWCas9 organoid line with doxycycline inducible expression of Cas9, was subjected to FACS to look at cas9 expression at different time points with doxycycline treatment. Doxycycline was added to the medium at a concentration of 0.5 µg/ml and the medium was replaced with/without doxycycline every two days. Orgaonids were collected in cell recovery solution, disrupted mechanically, and washed with cold PBS. They were then treated with 1ml Accutase solution for cellularization at 37°C for 10 minutes and washed with PBS. The organoid pellet was then fixed in PFA followed by immunostaining for Cas9 with Cas9 (7A9-3A3) mouse mAB (Alexa 647) (Cell Signalling) antibody and blocking with BSA.

Cell and organoid Culture.

Cell lines were maintained in DMEM + GlutaMax, supplemented with 10% foetal bovine serum and 1% PenStrep. Cells were passaged every 2-3 days and cultured at 37°C and 5%CO_2. For trypsinization of CMT93, 0.25% trypsin EDTA was used at 37°C for 10-15 mins. For trypsinization of HEK 293T cells, 0.05% trypsin-EDTA was used at 37°C for 5 mins. For transfections and transductions, cell medium without antibiotics was used.

APTK organoids were maintained in BME type 2 (R&D Systems) with medium containing Advanced DMEM F12 (Thermo Fisher Scientific; 12634-028), 1% penicillin/streptomycin (Thermo Fisher Scientific; 15140-22), 1× Glutamax (Thermo Fisher Scientific; 35050061), Hepes (Thermo Fisher Scientific; 15630056),1× N2 (Thermo Fisher Scientific; 17502–048), 1× B27 (Thermo Fisher Scientific; 17504-044), 80 µM N-acetylcysteine (Sigma-Aldrich; A9165), and 2 µg/ml Puromycin dihydrochloride. Organoids were passaged every 2-3 days and cultured at 37°C and 5%CO_2.

Softwares and statistical tests.

Graphpad Prism was used to plot qPCR data and perform statistical tests. Relative mRNA expression levels were determined from Ct values using the Delta Ct Ct or Livak's method. Parametric Unpaired T test and One way ANOVA was performed to verify statistical significance, where P value cutoff for significance was <=0.05.

Confocal imaging was performed on the CQ1 confocal microscope and visualised with ImageJ. Network interaction for *AGK* reported in literature were obtained by using genemania application in cytoscape software.

Chapter 3: Results.

1. Doxycycline induced expression of Cas9 does not vary temporarily and is not efficacious.

In order to determine the peak Cas9 expression post doxycycline induction in APTK-pCW_Cas9-Lenti_sgRNA_Puro organoids, organoids were subjected to doxycycline treatment for up to 14 days and the Cas9 expression was evaluated at various time points. Since the stably transduced population was not monoclonal, we opted to quantify Cas9 expression using FACS. Organoids at different time points were cellularised, fixed, and stained for Cas9 before subjecting to FACS. Data generated showed insignificant Cas9 expression and NO difference in Cas9 expression after long term Doxycycline treatment (Figure 5). Further, quantification of *AGK* knockout efficiency using RT-qPCR showed no significant difference between treated and untreated organoid lines. However there was a small but significant difference in AGK mRNA levels between knockout and control lines before Doxycycline induction, indicating possibility of a leaky promoter (Figure 6).

Figure 5: Quantification of Cas9 in APTK organoids post long term Doxycycline induction.

With Dr. Valentina Petrocelli

Line: APTK-pCW_Cas9-Lenti_***NMT***sgRNA-Puro

Day 0

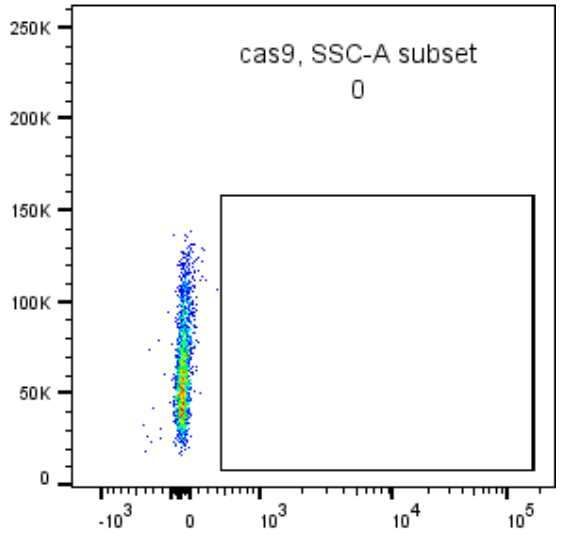

Day 3

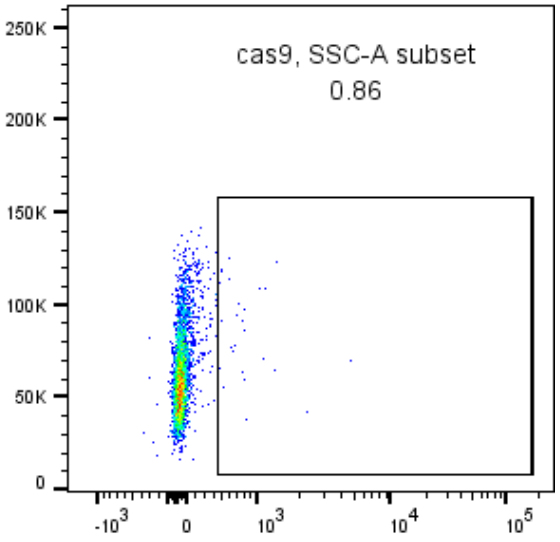

Day 7

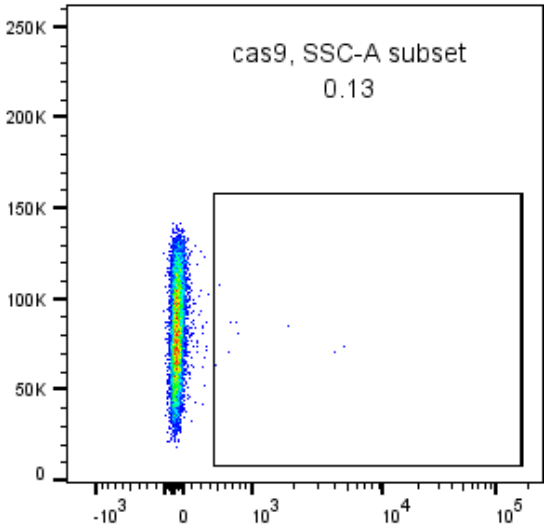

Day 10

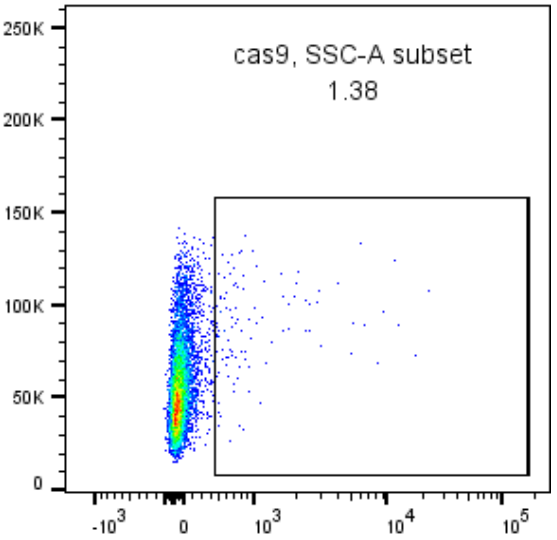

Day 14

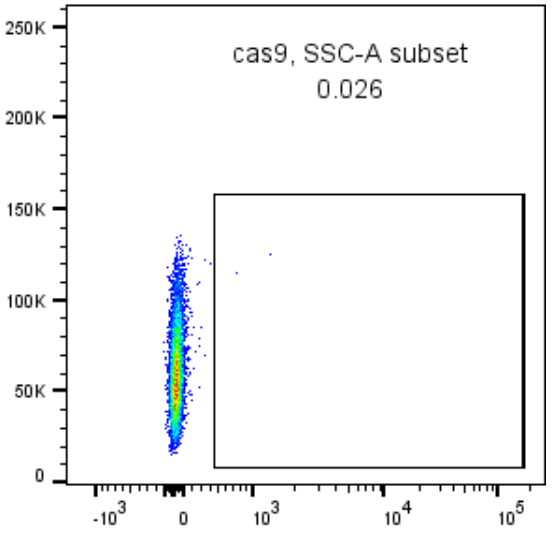

Line: APTK-pCW_Cas9-Lenti_***AGK***sgRNA-Puro

Day 0

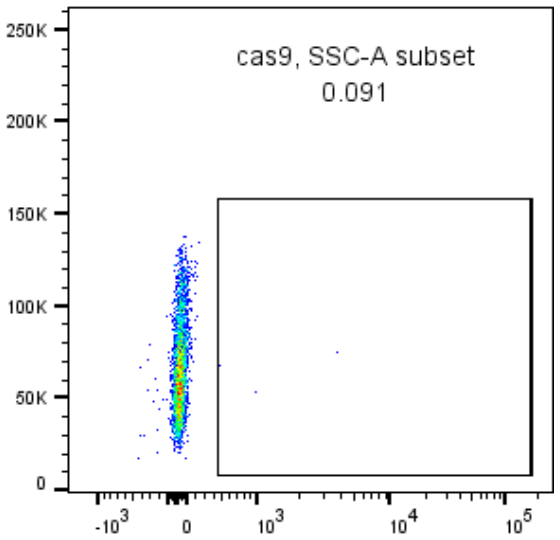

Day 3

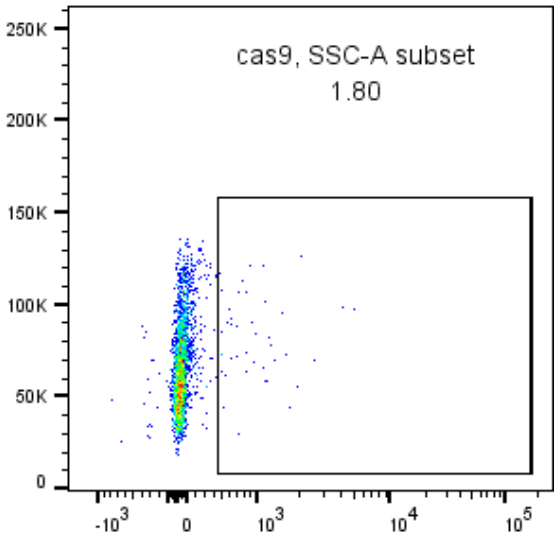

Day 7

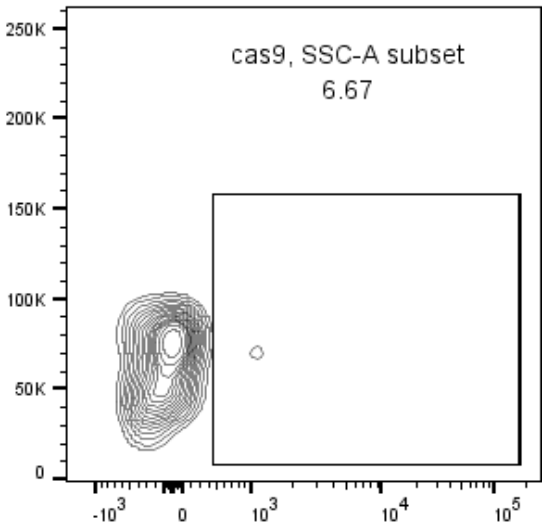

Day 10

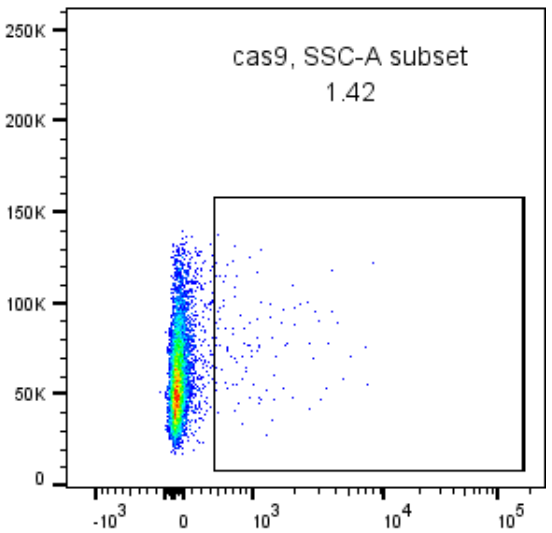

Day 14

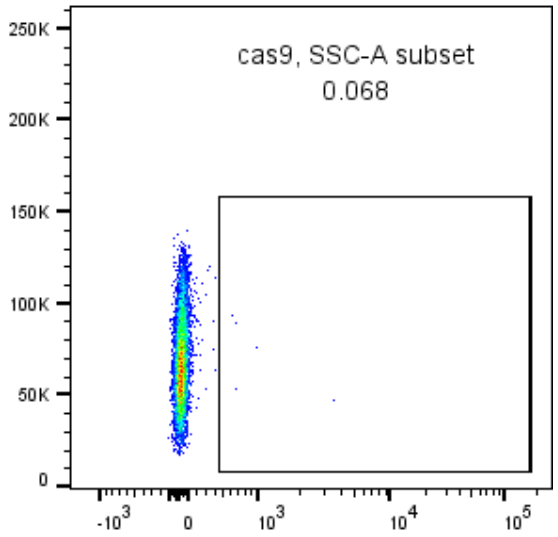

Description: Two APTK organoid lines (*AGK* knockout and *NMT* control) were subjected to FACS analysis for temporal expression of Cas9 upon long term Doxycycline induction. Cas9 expression does not vary significantly even upon long term exposure to doxycycline for both AGK knockout and control lines as indicated by the SSC-A subset that denotes percentage of cell population expressing Cas9.

This result was indicative of failure in successful transduction therefore we chose to quantify the knockout efficiency of previously generated lines in the lab. Data was quantified by RT-qPCR (Figure 6).

Figure 6: Quantification of *AGK* knockout efficiency in APTK organoids.

Lines generated by Dr. Marina Pesic.

A. Before Dox-Induction.

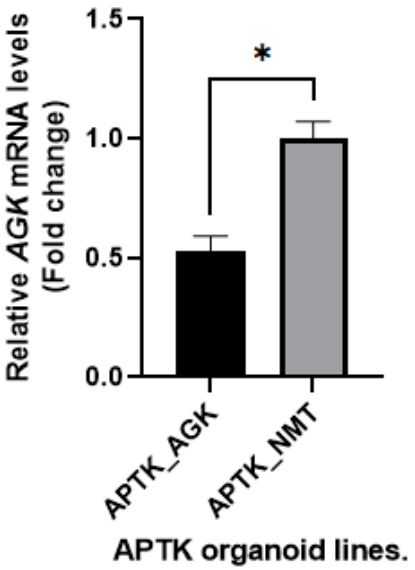

N = 2 ; Biological Replicates

n = 3 ; Technical Replicates

Reference Gene = *Ppia* (Cyclophilin).

Statistical test used = Unpaired T test (parametric)

P value = 0.0192

B. Post Dox induction for 2 Days.

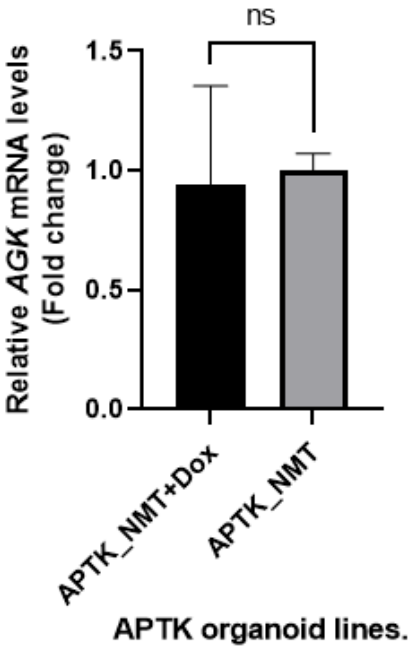

N = 2 ; Biological Replicates

n = 3 ; Technical Replicates

Reference Gene = *Ppia* (Cyclophilin).

Statistical test used = Unpaired T test (parametric)

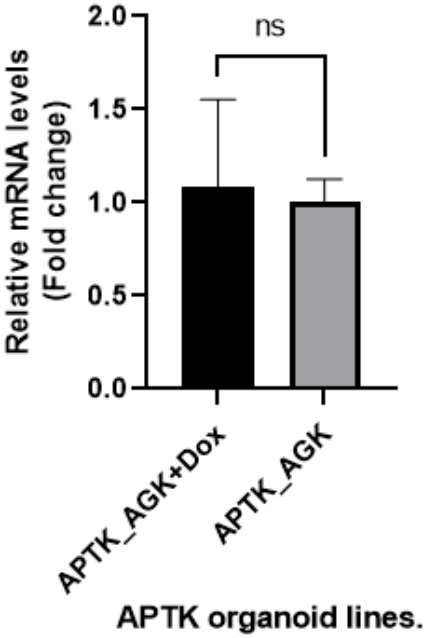

N = 2 ; Biological Replicates

n = 3 ; Technical Replicates

Reference Gene = *Ppia* (Cyclophilin).

Statistical test used = Unpaired T test (parametric)

Description: A. *AGK* knockout and *NMT* control APTK lines were quantified for *AGK* mRNA levels to test for knockout efficiency before doxycycline induction of Cas9 expression. This showed a significant difference between knockout and control lines even before dox induction. B. Both knockout and control lines were compared for AGK knockout efficiency before and after Dox induction. This showed no significant difference in expression of *AGK* mRNA levels in both knockout and control lines.
Dox; Doxycycline. *AGK*: Acyl glycerol Kinase. *NMT*: Control.

Taking into account the fact that the FACS data showed inefficient Cas9 expression across the timeline during the dox-induction in the lines generated by Dr. Valentina Petrocelli, and AGK knockout efficiency post Dox induction in the lines generated by Dr. Marina Pesic didn't show promising results, we sought to repeat the generation of APTK-pCW_Cas9 expressing organoids. However the organoids died during the selection process with blasticidin at day ~14. This suggested failure in transduction and therefore failure in

generation of stably transduced iCas9 expressing APTK organoids (Figure 7).

Figure 7: Negative data depicting failure in transduction of APTK organoids.

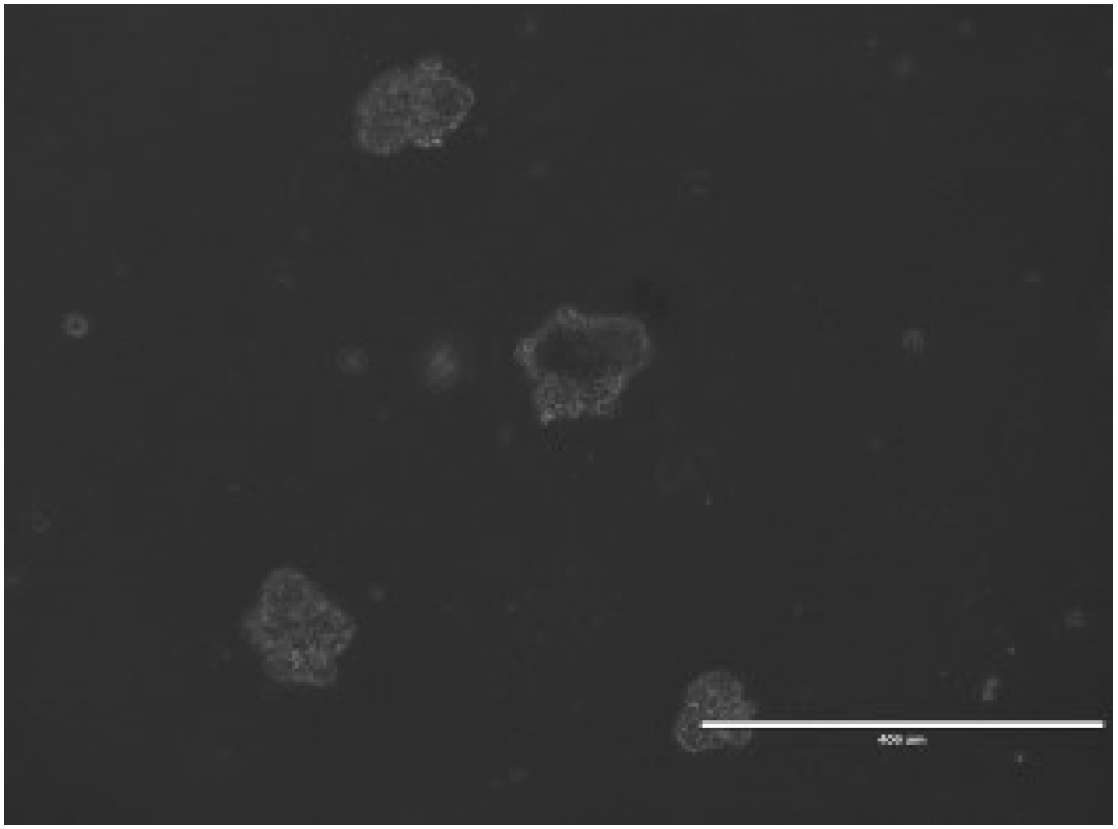

Description: Figure depicts dead organoid after selection with blasticidin. They showed characteristics of apoptotic cells, such as fragmented and shrunken appearance, small size, and dark appearance under Bright field microscope with lack of growth.

The aforementioned data along with data generated in the lab by other members suggested error/s in the very initial experiments of the experimental workflow design, that is transfections and transductions. Therefore we focused on improving the viral titre and transfection efficiencies. It is known that the amount of functional viral titer produced and efficiency of transection, both depend on the transfection reagent used. Therefore we tried to optimise

the aforementioned by trying out three different transfection reagents. Lentiviral concentration was performed using three methods, 1. Overnight centrifugation at 10,000 g. 2. Centrifugation at 25,000g for 2 hours, and 3. Usage of Vivaspin 6, 10kDa, MWCO Polyethersulfone columns. Concentration of functional lentiviral titre was maximised with Vivaspin columns, as reported in literature(Pirona *et al.*, 2020) and therefore for downstream concentration of lentiviruses, vivaspin columns were used.

2. Troubleshoot Data:

a. Lipofectamine shows the highest transfection efficiency.

We tried to optimise the molar ratios of the three plasmids (Transfer vector plasmid and two packaging plasmids) for optimal transfections using three different transfection reagents, namely lipofectamine, Polyjet and Calcium chloride in HBS buffer and found that Lipofectamine shows the highest transfection efficiency (Figure 8). It is known that the transfection efficiency reduces with increase in vector size and many reagents show similar efficiencies with smaller vectors therefore we compared the transfection efficiency by using a big vector (SCAR-Cas9-blast: 13.3 Kb). Since it was required to use the SCAR vector due to the possibility of a leaky iCas9 promoter in pCW-Cas9 plasmid, using SCAR-Cas9-Blast for the troubleshoot experiments was a relevant choice. Moreover, data generated by Dr. Valentina Petrocelli showed very poor transfection efficiencies with SCAR vector, therefore it was imperative to improve upon the transfection efficiencies for the SCAR vector.

Figure 8: Transfection efficiencies with different transfection reagents.

A. Lipofectamine.

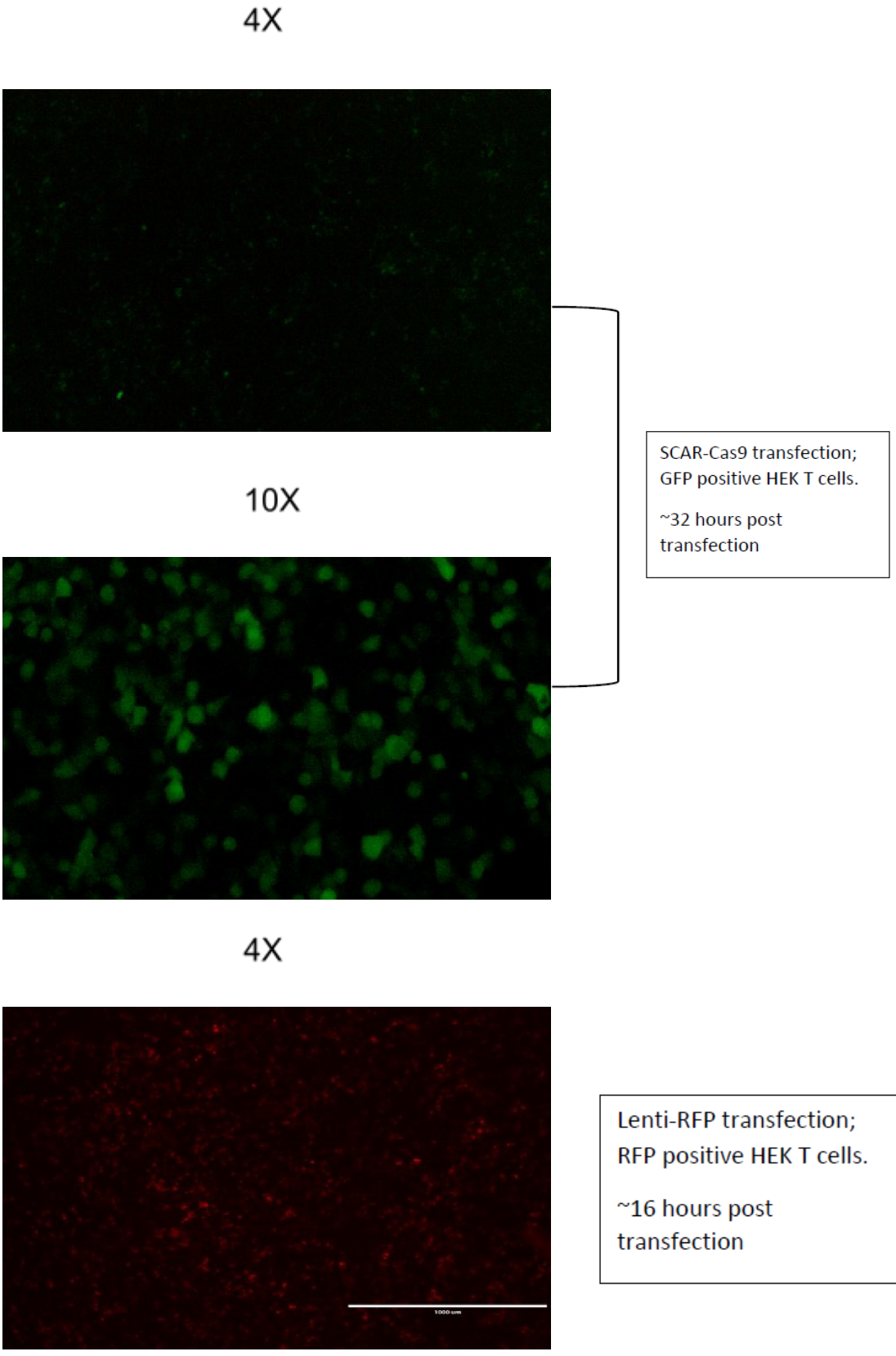

B. Polyjet and Calcium Chloride in HBS Buffer.

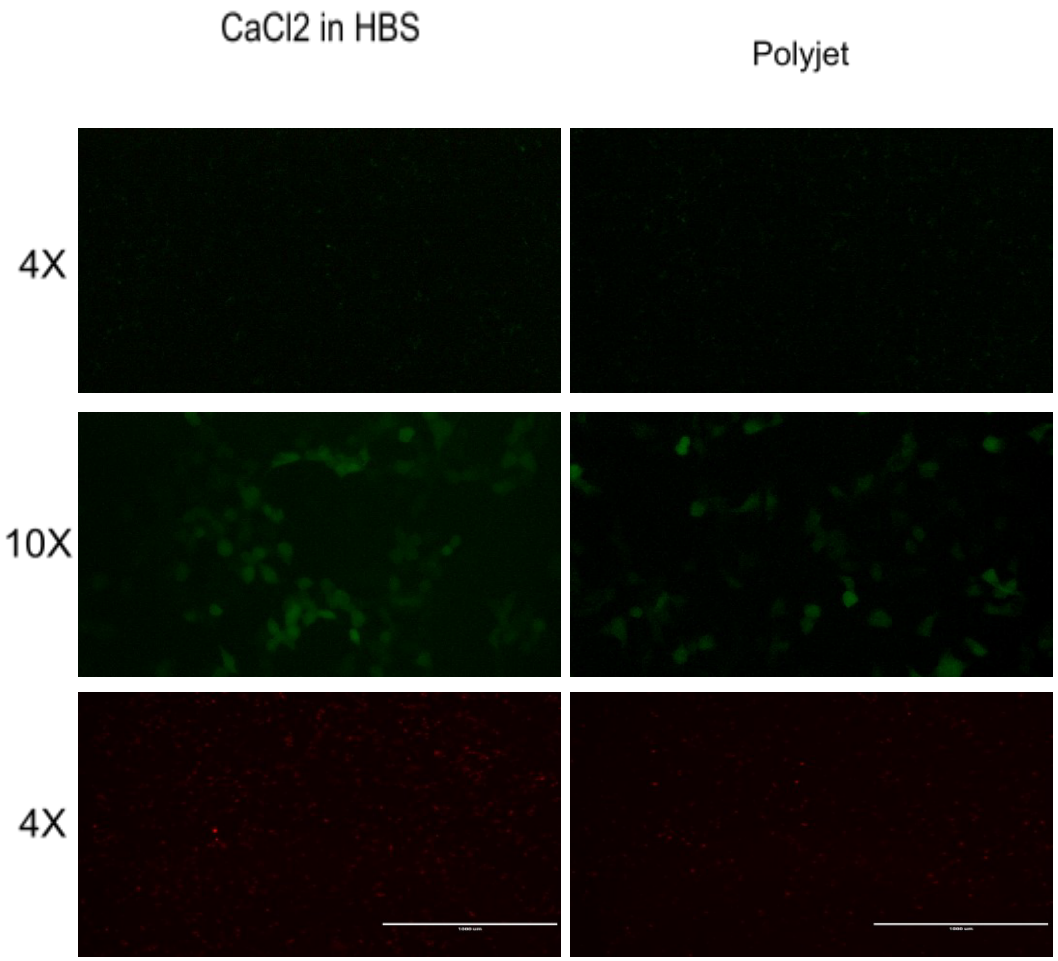

Description: HEK 293T cells were transfected with three transfection reagents (**A**; Lipofectamine, **B**; Calcium chloride in HBS buffer and Polyjet). GFP positive cells are indicative of successful transfection with SCAR-Cas9 vector (13.3 Kb) RFP positive cells are indicative of successful transfection with Lenti-RFP vector (~6Kb). These results show difference in transfection efficiency with difference in vector size as well as with different transfection reagents. Lipofectamine shows maximum transfection efficiency in both cases. 4X, 10X: Magnification scales, GFP; Green fluorescent protein, RFP: Red fluorescent protein.

Despite the achievement of desired transfection efficiency and efficient functional lentiviral titre concentration , we observed complete failure in transductions with both CMT 93 cell line and APTK organoids. Therefore, we sought to check the plasmid constructs used in these aforementioned experiments for recombination or any other defect that was leading to failure in transduction events.

b. Recombination in pMD2.G plasmid.

For this plasmids were digested with restriction enzymes and were subjected to gel electrophoresis (Figure 9). The generated Data showed recombination in the pMD2.G plasmid that encodes for the envelope proteins of the lentivirus, that are imperative for successful infections. Undigested circular plasmids when run on agar gel show 3 bands, while linearised plasmids show a single band upon digestion with one enzyme with a single site in the construct.

Figure 9: Gel electrophoresis data depicting possible recombination in pMD2.G plasmid.

A.

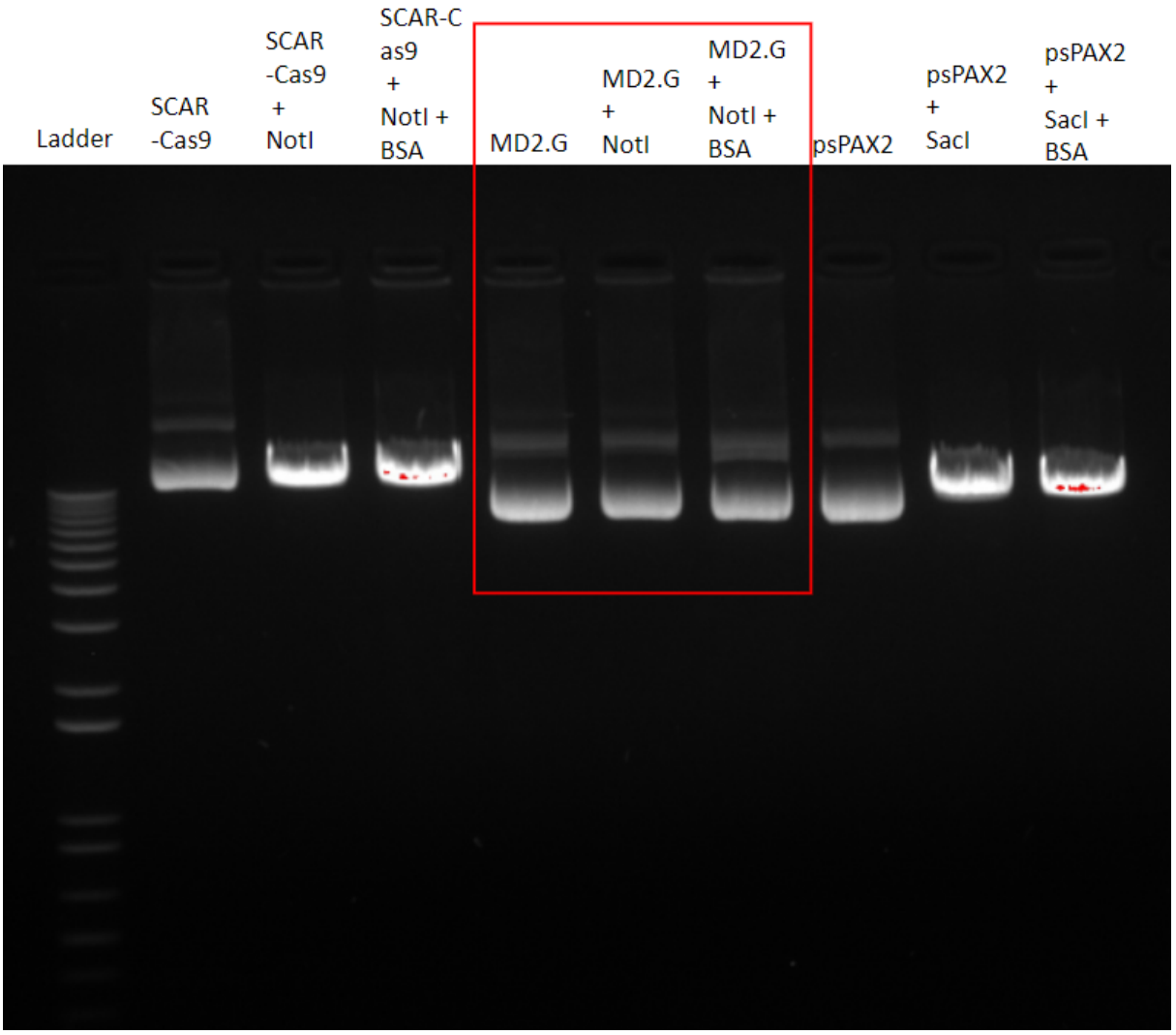

B.

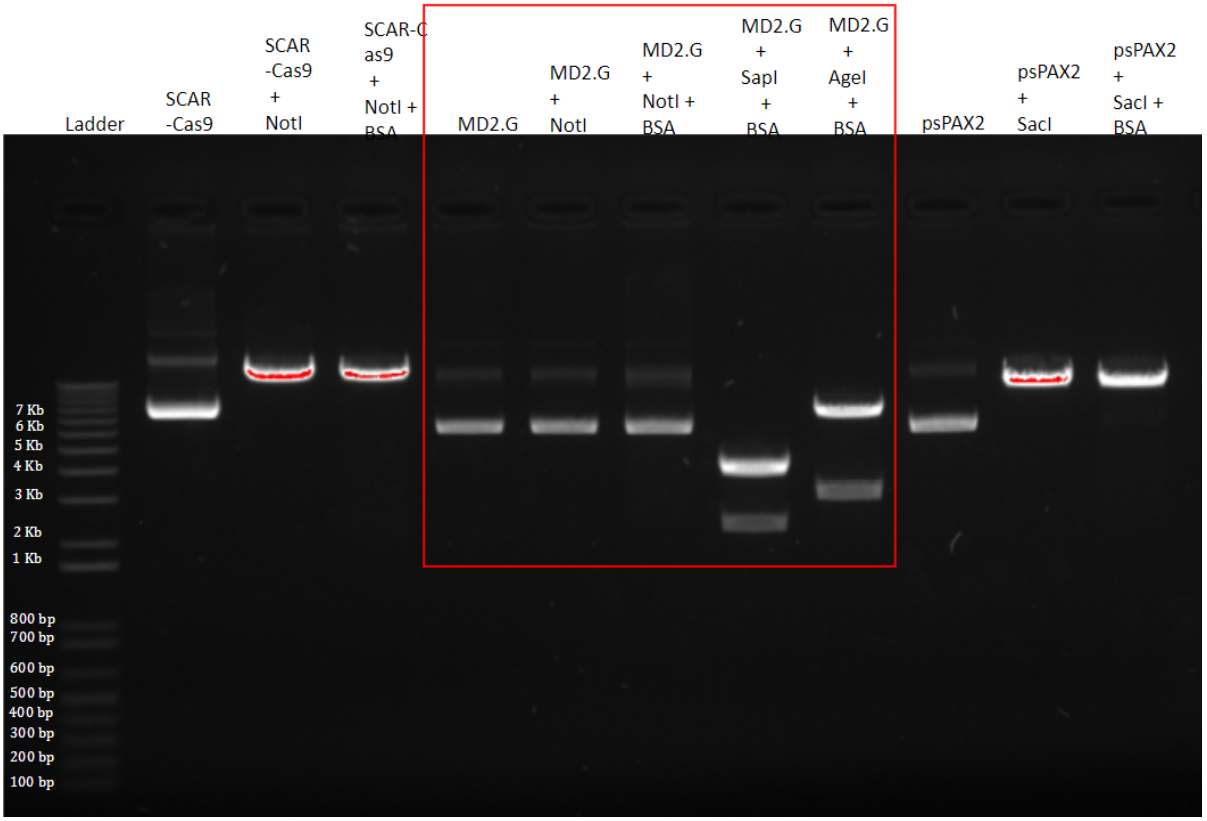
Ladder
SCAR -Cas9
SCAR -Cas9 + NotI
SCAR-Cas9 + NotI + BSA
MD2.G
MD2.G + NotI
MD2.G + NotI + BSA
MD2.G + SapI + BSA
MD2.G + AgeI + BSA
psPAX2
psPAX2 + SacI
psPAX2 + SacI + BSA
7 Kb
6 Kb
5 Kb
4 Kb
3 Kb
2 Kb
1 Kb
800 bp
700 bp
600 bp
500 bp
400 bp
300 bp
200 bp
100 bp

C.

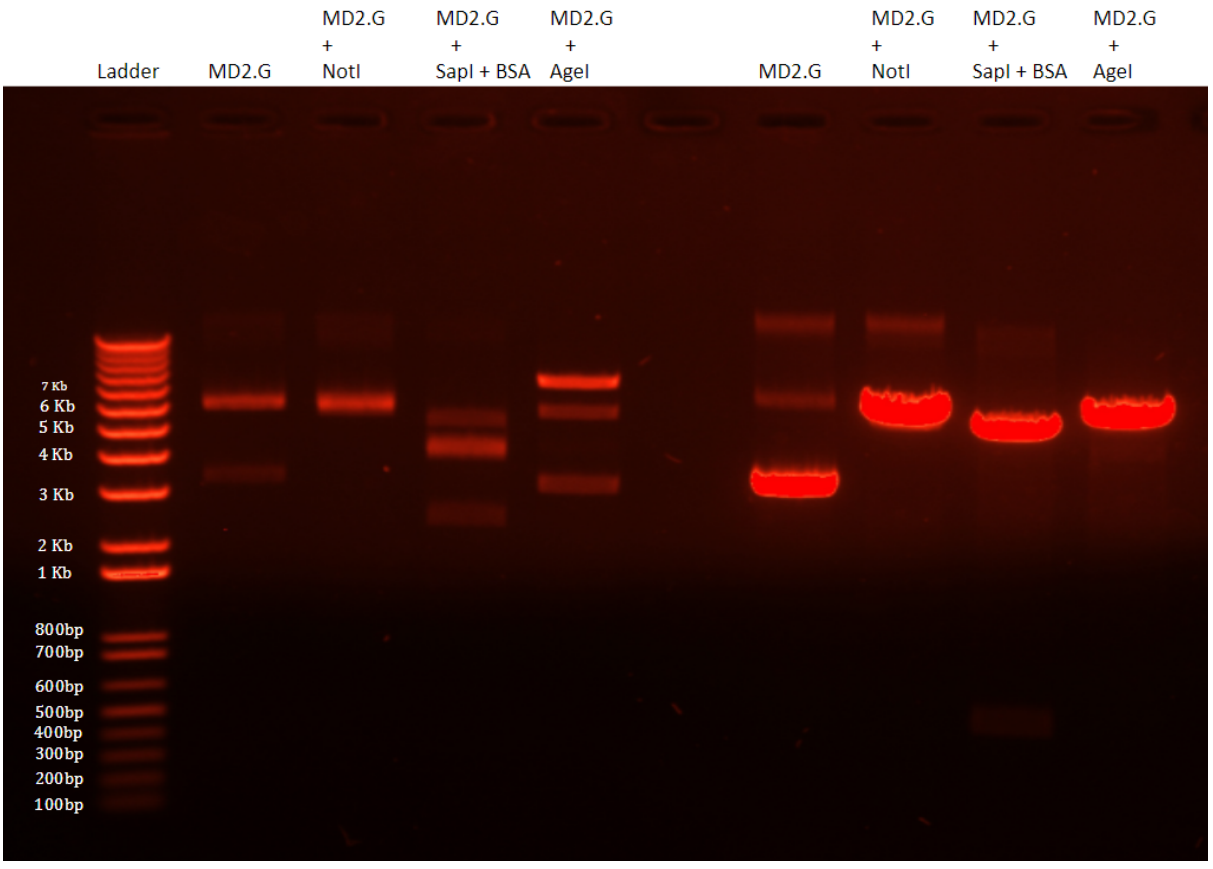
Ladder
MD2.G
MD2.G + NotI
MD2.G + SapI + BSA
MD2.G + AgeI
MD2.G
MD2.G + NotI
MD2.G + SapI + BSA
MD2.G + AgeI
7 Kb
6 Kb
5 Kb
4 Kb
3 Kb
2 Kb
1 Kb
800bp
700bp
600bp
500bp
400bp
300bp
200bp
100bp

Description: **A.** pSCAR-Cas9, pMD2.G, and psPAX2 vectors were digested with NotI, NotI and Sac1 restriction enzymes respectively. For each vector, an undigested plasmid was also run on the gel. In concordance with the literature, the undigested plasmid shows three bands as expected. In the case of pSCAR-Cas9 and psPAX2 vectors, linearised plasmids digested with a single restriction enzyme show a single bright band at appropriate loci. In the case of pMD2.G, both digested and undigested samples show the exact same pattern as expected in undigested samples, when subjected to gel electrophoresis. **B.** As mentioned before, pSCAR-Cas9 and psPAX2 vectors are treated with the same restriction enzymes. pMD2.G is treated with a total of 3 restriction enzymes, Not1, SapI, and AgeI, individually, that is one enzyme per sample. In concordance with A., pSCAR-Cas9 and psPAX2 show the expected band pattern in digested and undigested samples. However pMD2.G shows two linearised bands when digested with Sap1 and AgeI. **C.** Two samples of pMD2.G obtained from two different sources in the lab were treated with the same three restriction enzymes, Not1, Sap1, and Age1. Left hand side sample shows an aberrant ectopic band pattern upon restriction-enzyme digestion whilst the right hand side sample shows the expected band pattern observed in undigested and digested samples.

This data clearly demonstrated there were very high chances that all the previous experiments were failing due to failure of transduction. Therefore we sought to repeat all the experiments with a new sample of pMD2.G obtained that showed the correct band pattern as seen in the case of pSCAR-Cas9 or psPAX2 vectors.

3. Cloning of sgRNA oligos in SCAR vector.

We cloned the various sgRNA oligos for AGK , NMT and PDL1 into the SCAR and validated the results with sequencing. The sgRNA construct was cloned using the BsmB1 restriction enzyme into the SCAR vector wherein the expression cassette

was under the U6 promoter. Figure 9 shows the sequencing validation of the cloning results. These cloned samples were then used to transform NEB *E.coli* bacteria and cultured for maxi preps.

Figure 10: Sequencing validation of cloning reaction results of sgRNA oligos for *AGK*, *PDL1* and *NMT* in the SCAR vector.

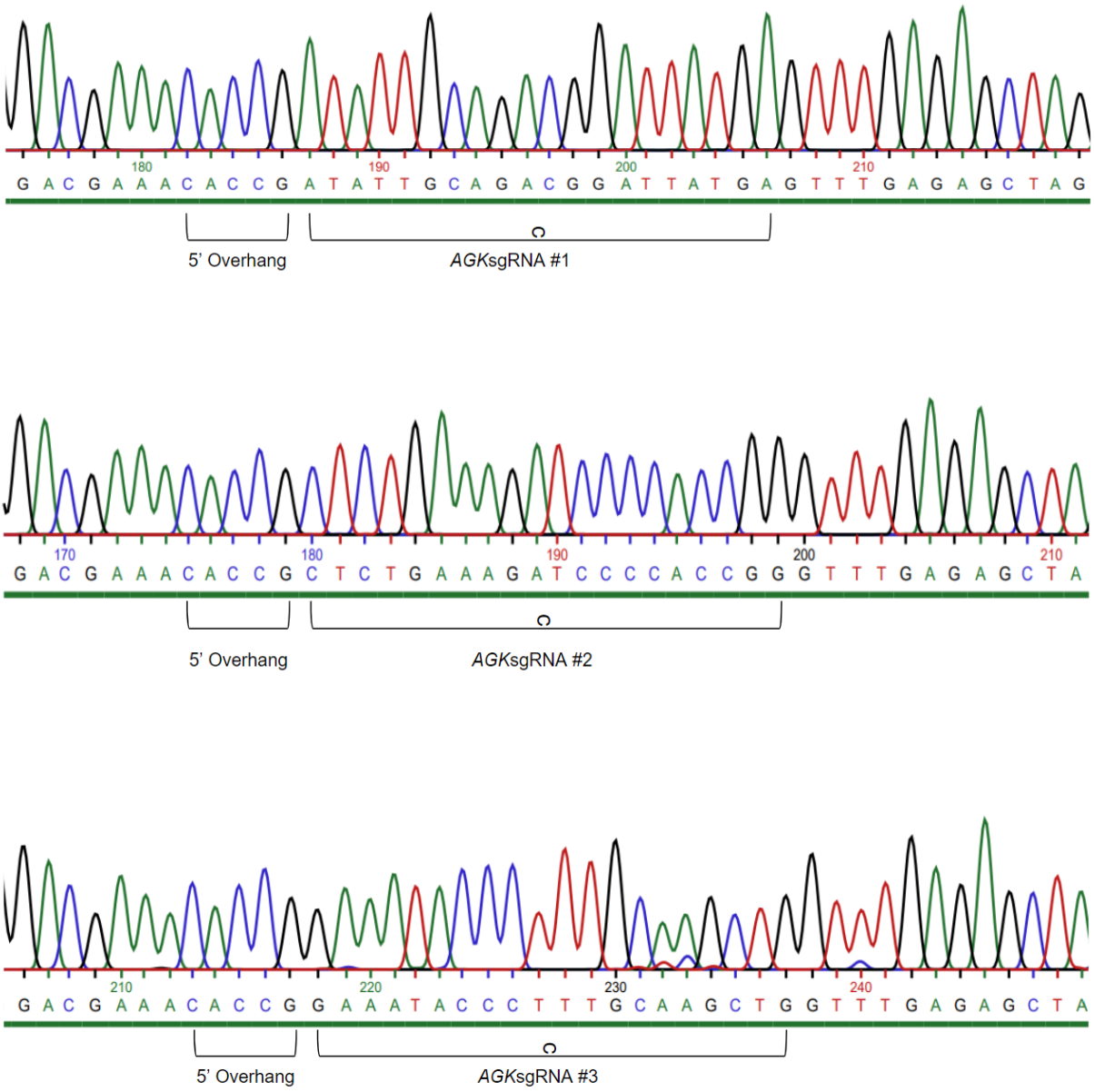

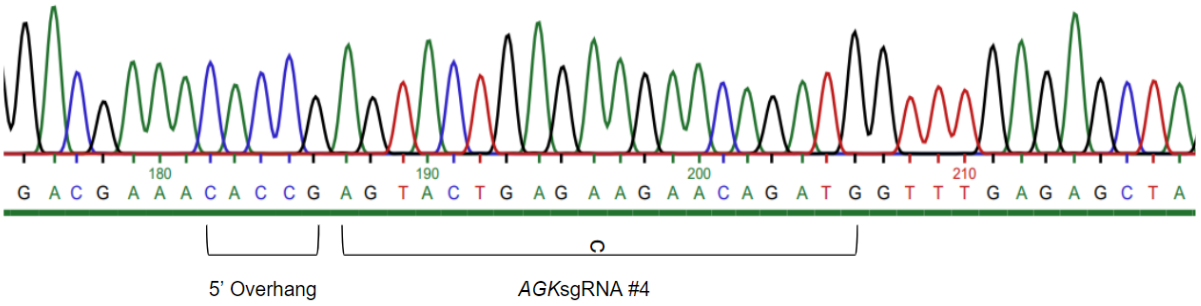
180
190
200
210
G A C G A A A C A C C G A G T A C T G A G A A G A A C A G A T G G T T T G A G A G C T A
5' Overhang
AGKsgRNA #4

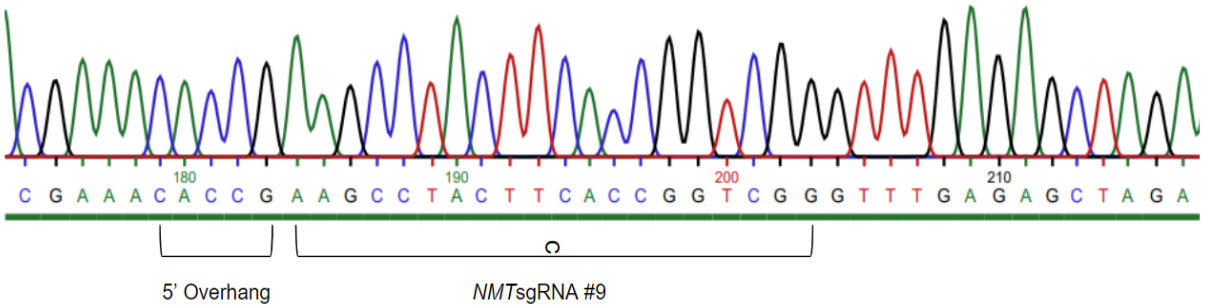
180
190
200
210
C G A A A C A C C G A A G C C T A C T T C A C C G G T C G G G T T T G A G A G C T A G A
5' Overhang
NMTsgRNA #9

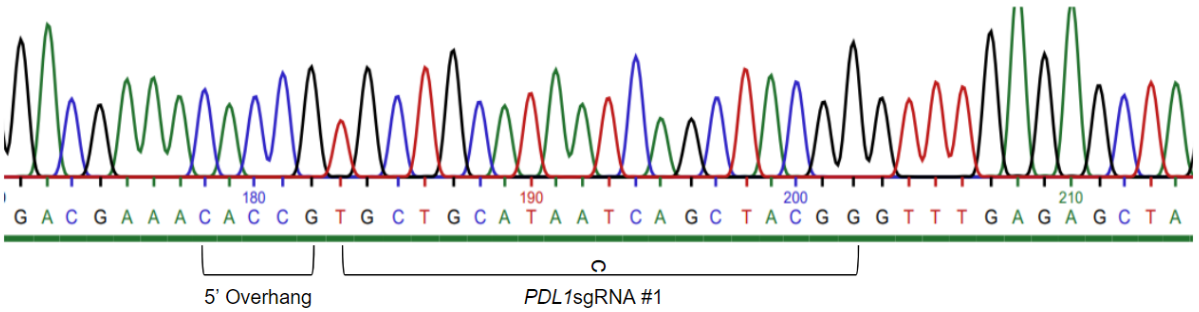
180
190
200
210
G A C G A A A C A C C G T G C T G C A T A A T C A G C T A C G G G T T T G A G A G C T A
5' Overhang
PDL1sgRNA #1

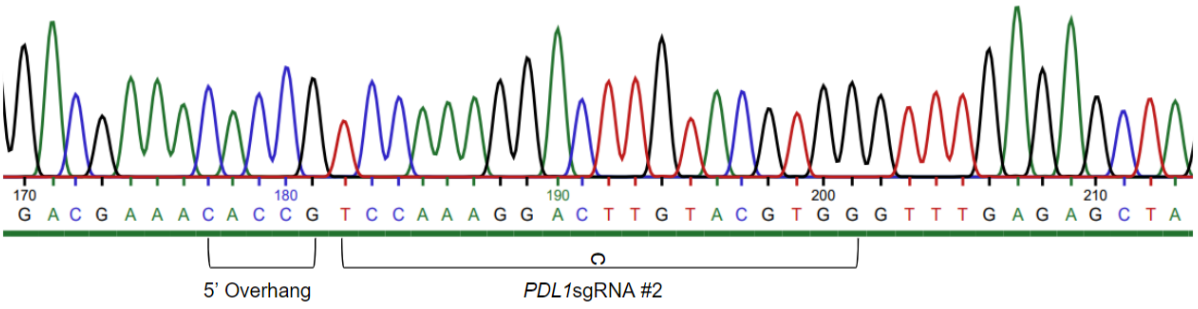
170
180
190
200
210
G A C G A A A C A C C G T C C A A A G G A C T T G T A C G T G G G T T T G A G A G C T A
5' Overhang
PDL1sgRNA #2

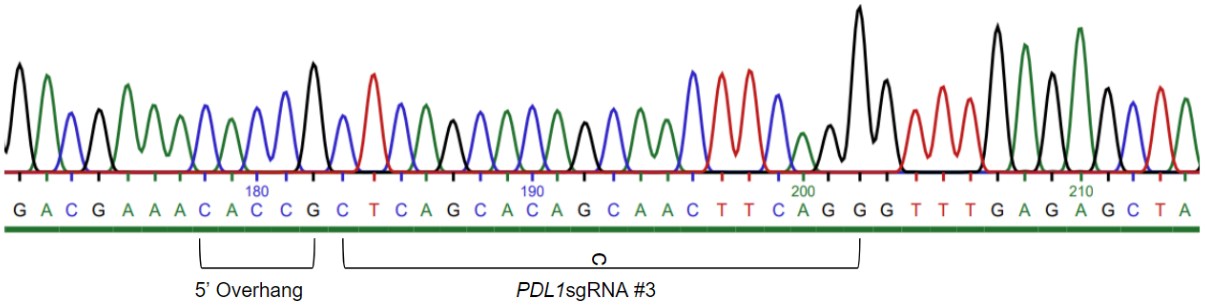

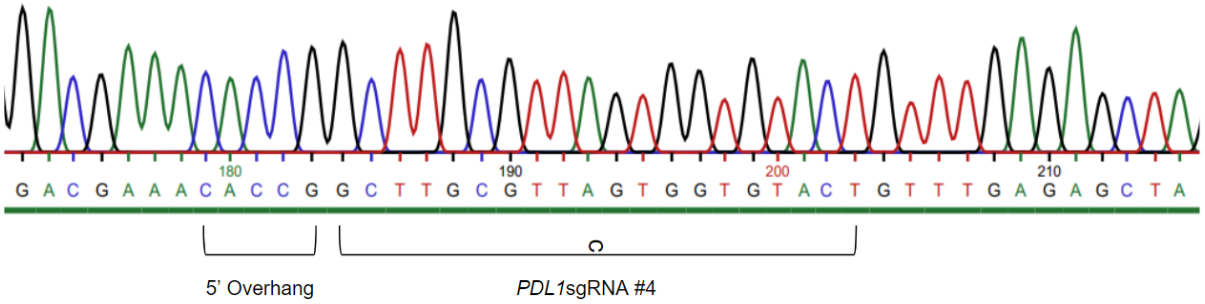

---

4. Generation of stably transduced APTK organoid lines with SCAR vector.

APTK organoids were first transduced (Post lentivirus generation) with SCAR-Cas9 vector (GFP tag). These organoids post-selection with blasticidin were transduced with SCAR-sgRNA vector (BFP tag) and double positive organoids were selected with hygromycin and blasticidin (Figure 10). These lines were quantified for Cas9 and AGK knockout efficiency using RT-qPCR method (Figure 11).

Figure 11: Stably tranduced APTK organoid lines.

A.

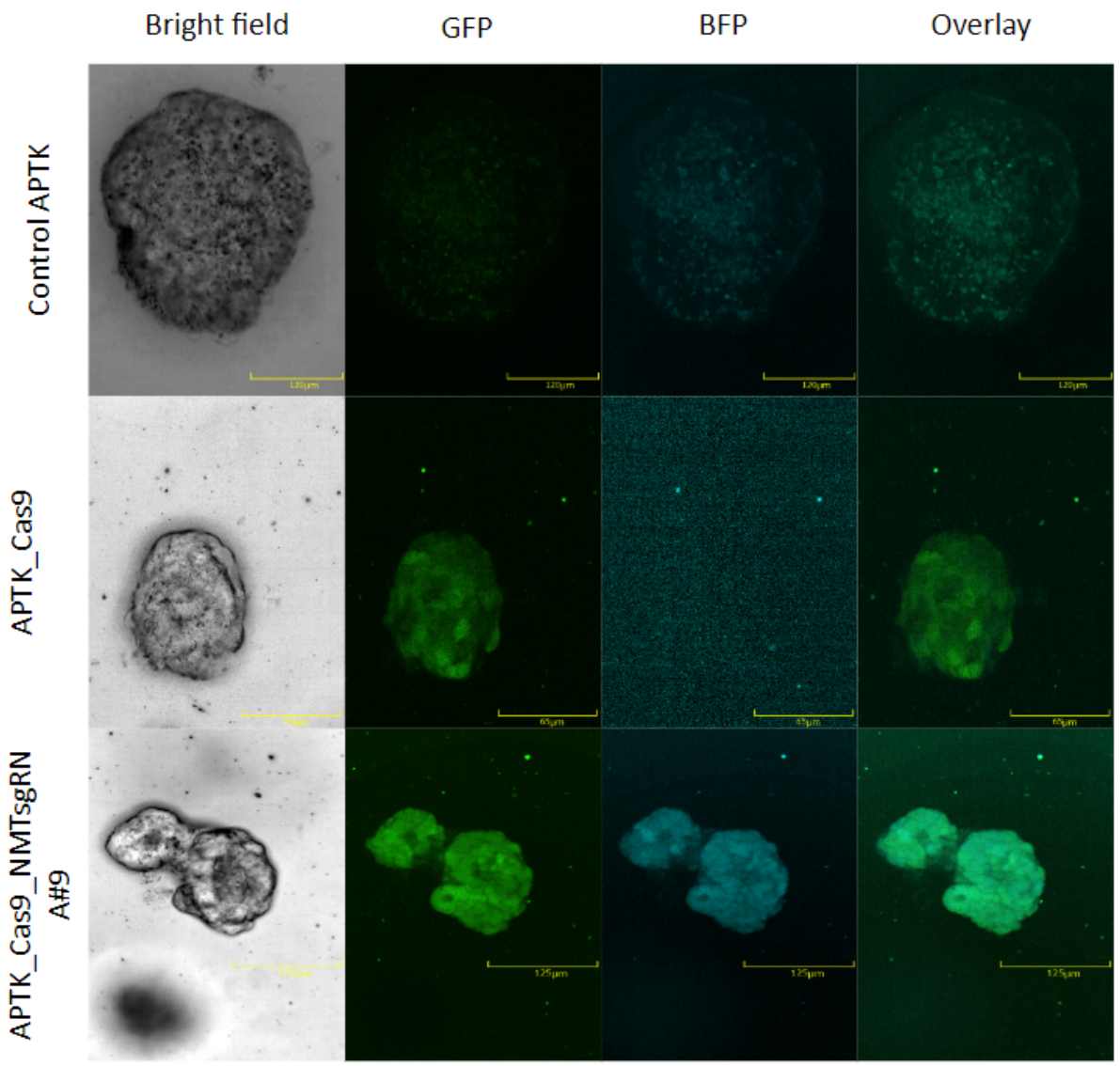

B.

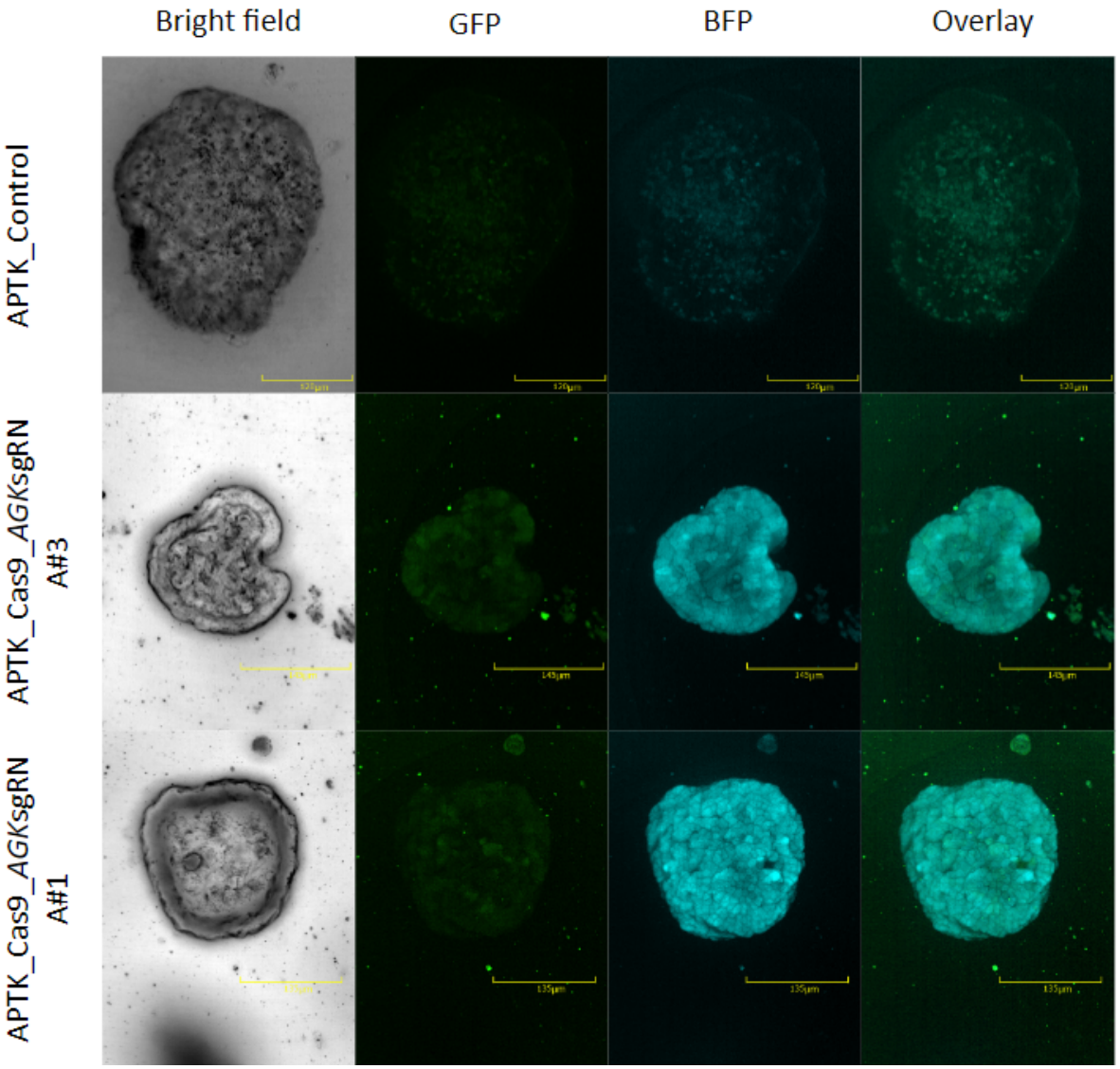
Bright field
GFP
BFP
Overlay
APTK_Control
APTK_Cas9_AGKsgRN A#3
APTK_Cas9_AGKsgRN A#1

C.

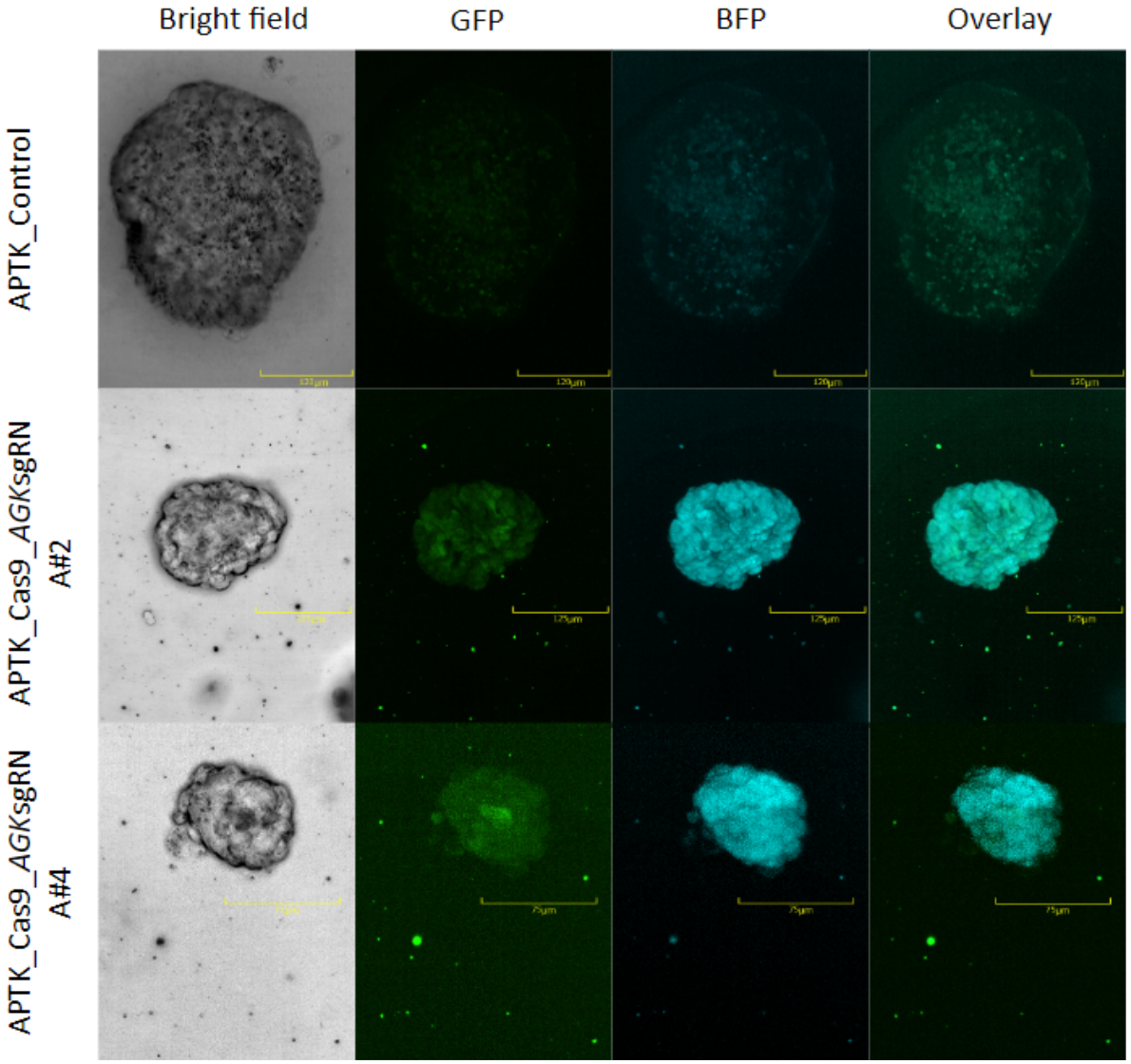
Bright field
GFP
BFP
Overlay
APTK_Control
APTK_Cas9_AGKsgRN A#2
APTK_Cas9_AGKsgRN A#4

Description: Control organoids as shown in the top row panel do not show GFP or BFP signal. Apoptotic cells show autofluorescence as seen in the panels. 4 different lines for AGK with different sgRNAs (#1 - #4) were used. SCAR-Cas9 vector has blasticidin resistance and GFP as reporter proteins and SCAR-sgRNA vector has hygromycin resistance and BFP tag as reporter proteins. Double positive organoids are both GFP and BFP positive as seen in the overlay column in the panels.
GFP: Green Flourescent protein, BFP: Blue fluorescent protein.

Figure 12: Quantification of stably transduced APTK lines.

A.

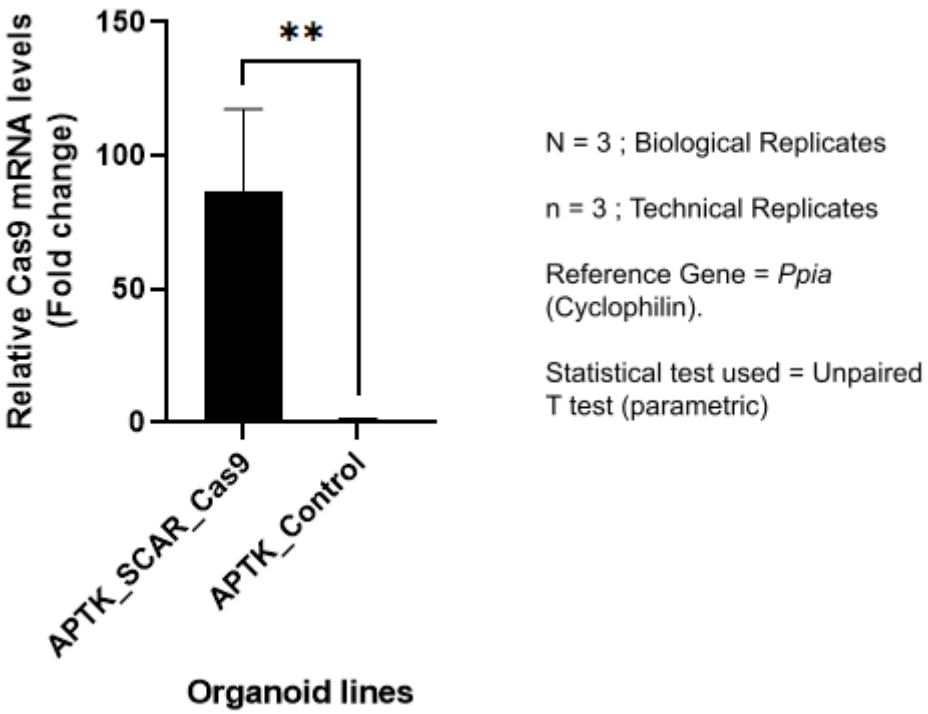

B.

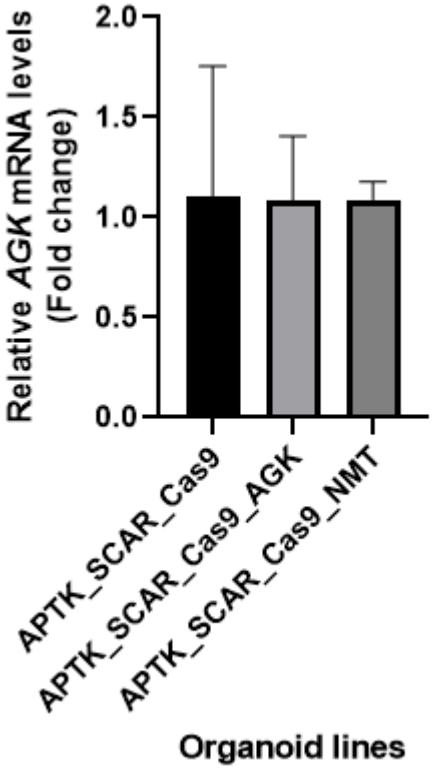

ANOVA summary

F: 0.001256

P value: 0.9987

P value summary: ns

5. Generation of stably transduced CMT-93 cell lines with SCAR vector.

CMT-93 cell line was first transduced (Post lentivirus generation) with SCAR-Cas9 vector (GFP tag). These cells post-selection with blasticidin were transduced with SCAR-sgRNA vector (BFP tag) and double positive organoids were selected with hygromycin and blasticidin (Figure 12). These lines were quantified for Cas9 and PDL1 knockout efficiency using RT-qPCR method (Figure 13). Stably transduced cell lines were subjected to limiting dilution for generation of monoclonal populations and 3 clones were quantified for PDL1 knockout efficiency (Figure 14).

Figure 13: Stably tranduced CMT-93 cell lines

A.

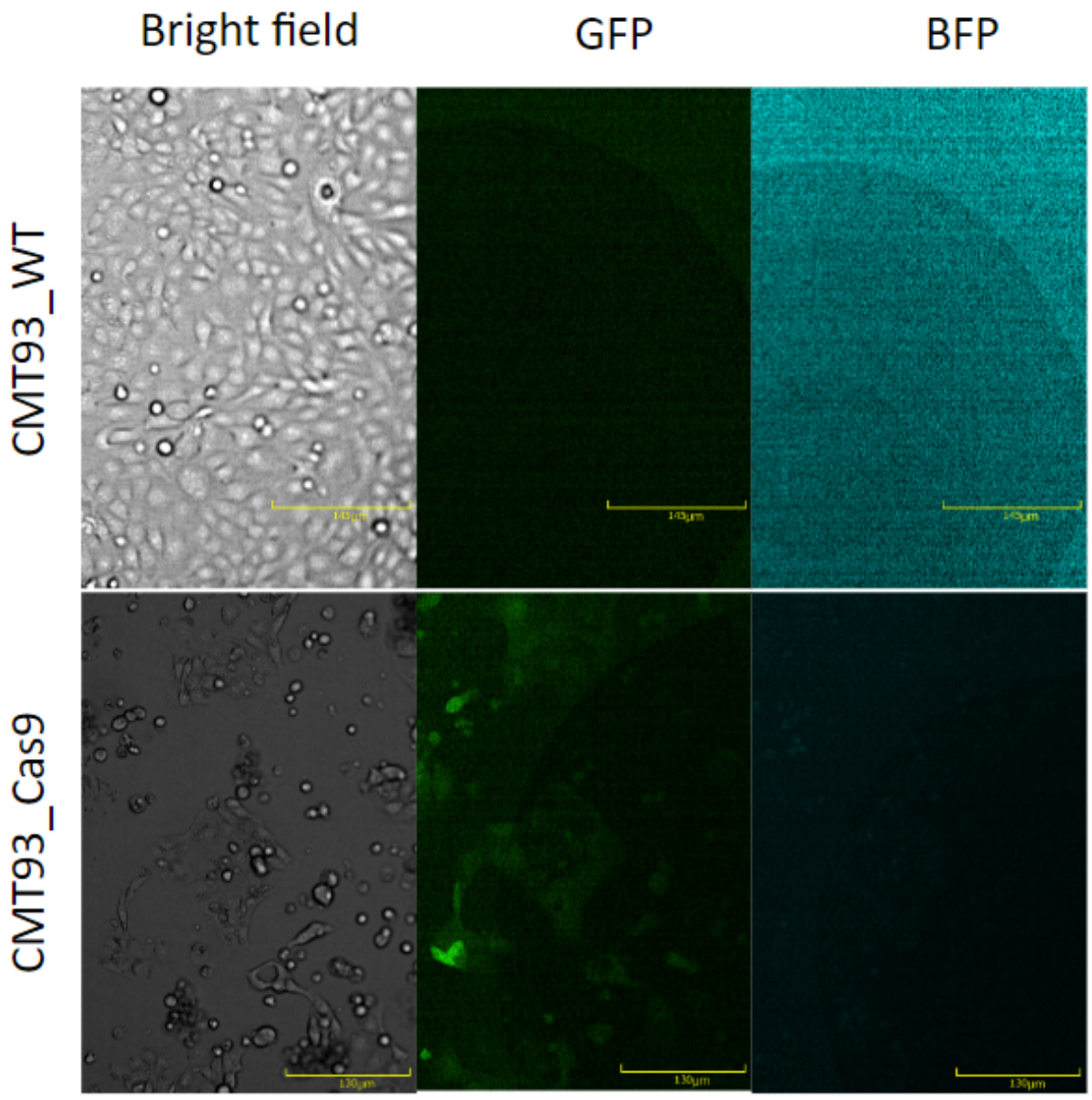

B.

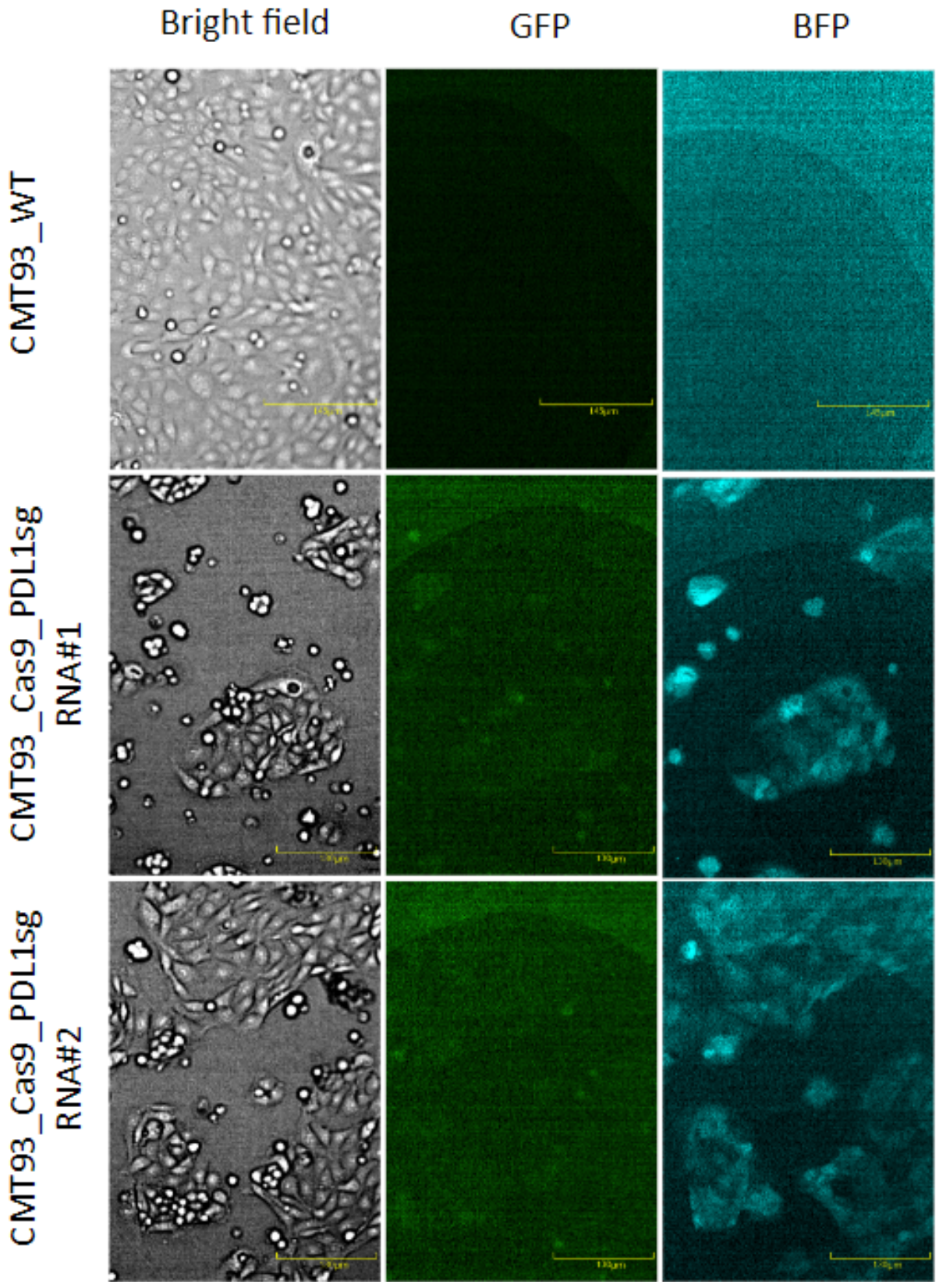
Bright field
GFP
BFP
CMT93_WT
CMT93_Cas9_PDL1sg RNA#1
CMT93_Cas9_PDL1sg RNA#2

C.

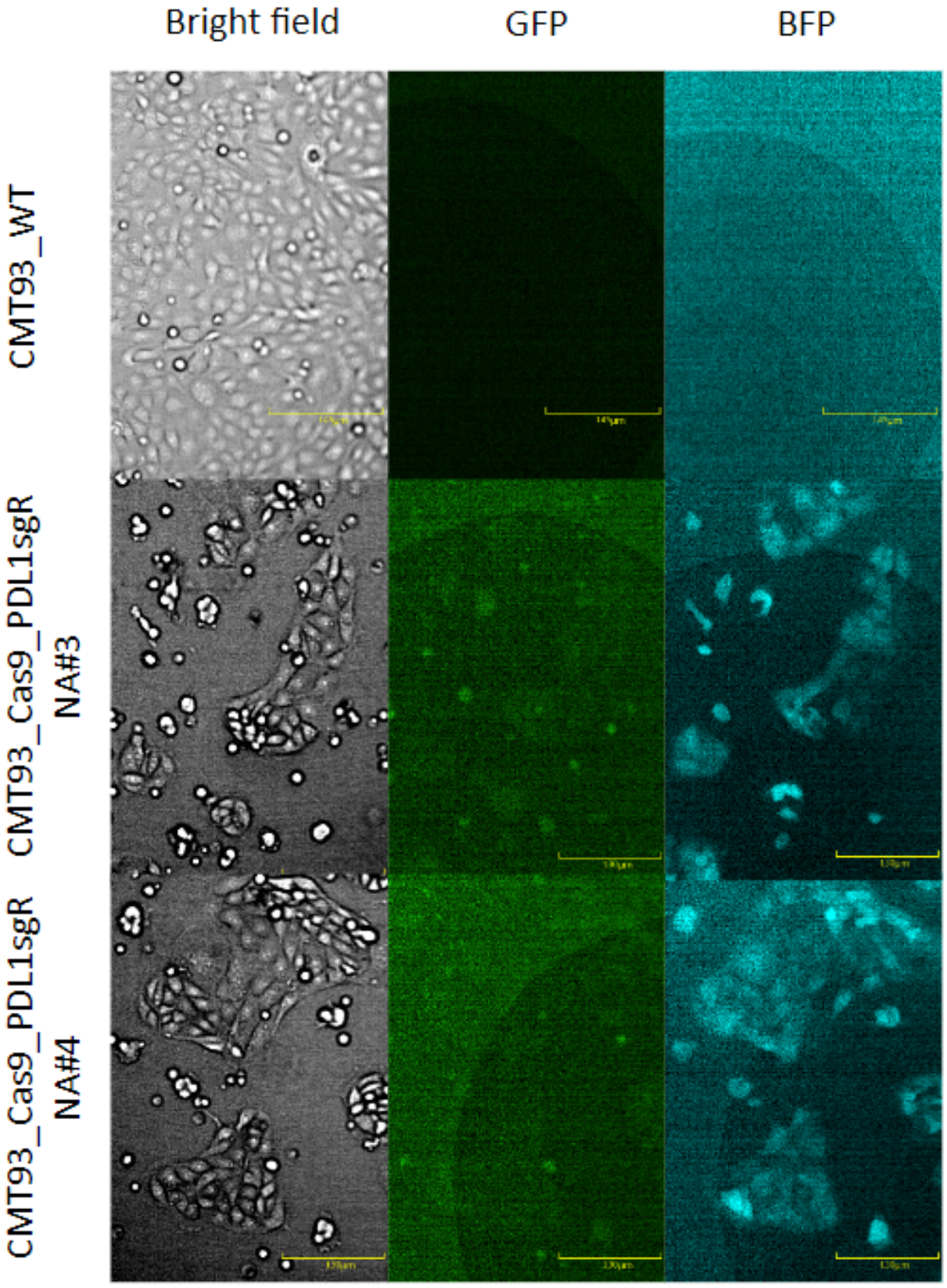
Bright field
GFP
BFP
CMT93_WT
CMT93_Cas9_PDL1sgR NA#3
CMT93_Cas9_PDL1sgR NA#4

Description: Control CMT-93 cell line (CMT-93 _WT) as shown in the top row panel do not show GFP or BFP signal. Apoptotic cells show autofluorescence as seen in the panels. 4 different lines for PDL1 with different sgRNAs (#1 - #4) were used. SCAR-Cas9 vector has blasticidin resistance and GFP as reporter proteins and SCAR-sgRNA vector has hygromycin resistance and BFP tag as reporter proteins. Double positive cells are both GFP and BFP positive as seen in the overlay column in the panels.

GFP: Green Flourescent protein, BFP: Blue fluorescent protein.

Figure 14: Quantification of stable transduced CMT-93 Cell lines.

A.

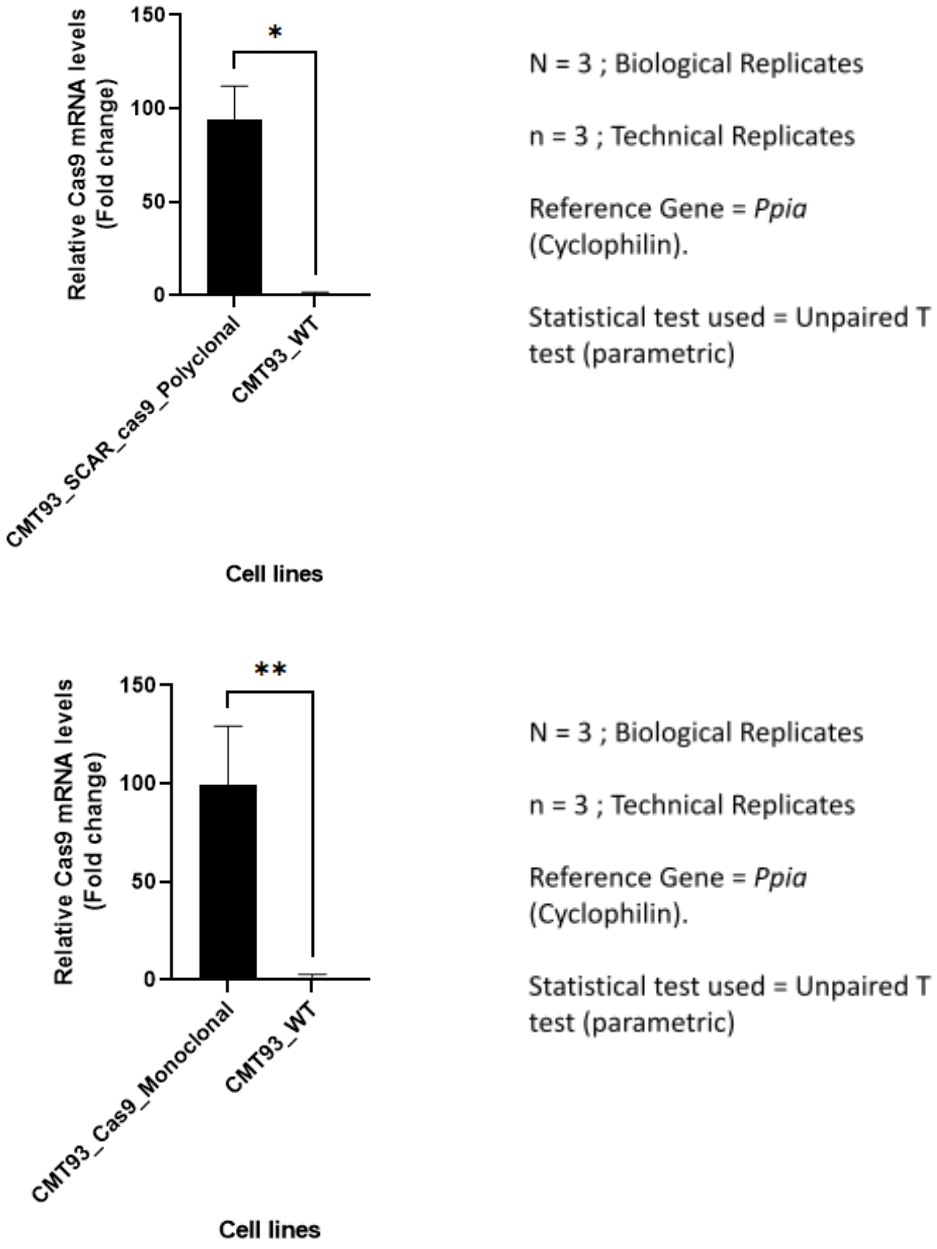

B.

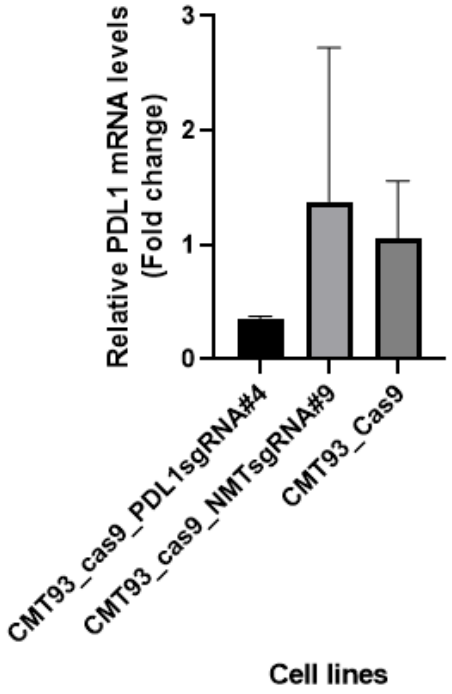

ANOVA summary

F: 0.8120

P value: 0.5226

P value summary: ns

Figure 15: Quantification of Monoclonal clones of CMT93-Cas9-*PDL1*sgRNA line for PDL1 knockout.

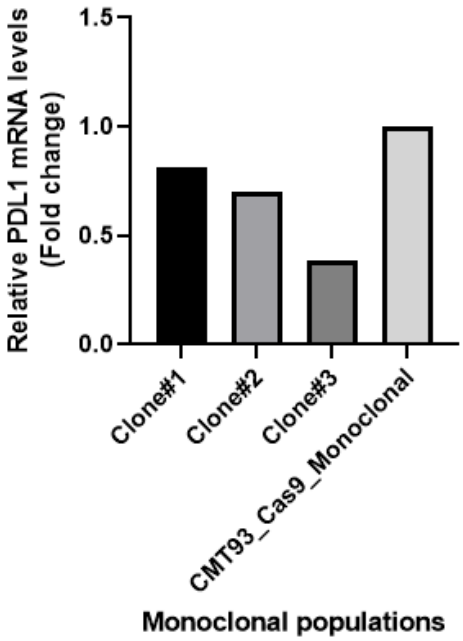

N = 1 ; Biological Replicates

n = 3 ; Technical Replicates

Reference Gene = *Ppia* (Cyclophilin).

Statistical test used = None

Description: Clone #1 - #3 are monoclonal populations derived from the polyclonal CMT-93-Cas9-PDL1sgRNA#4 line. Their quantification for PDL1 knockout shows variation between clones when normalised to control (CMT-93 Cas9_monoclonal) line as indicated by difference in relative PDL1 mRNA levels.

Chapter 4: Discussion.

In this thesis we attempted to validate the role of *AGK* knockout as a potential therapeutic target for immune checkpoint blockade therapy in colorectal cancer using APTK organoids as model system whilst aiming to overcome a major drawback of the previous screen that was performed in the lab. The main drawback was that of induced immunogenicity *in vivo* against foreign proteins like Cas9 and antibiotic resistance proteins, etc which continued to express post transplantation of genetically modified organoids/cell lines in mice. *AGK* or acyl glycerol kinase is a mitochondrial lipid kinase involved in promotion of tumorigenesis via increased production of LPA, when upregulated in tumor cells. AGK plays both kinase dependent and kinase independent functions and contributes to tumorigenesis.

In order to investigate the aforementioned asked question we employed two approaches to generate genetically modified APTK organoids, one which involved usage of SCAR vector and one that involved taking advantage of the inducible promoter under which Cas9 was expressed (pCW-Cas9 vector). Both of these approaches ultimately involved *in vitro* gene editing and transplantation of the gene edited population in mice. In order to determine the optimal amount of Cas9 expression sufficient to obtain gene knockout, APTK organoids expressing pCW-Cas9 were generated with Dr. Valentina Petrocelli which were then subjected to long term doxycycline treatment for induction of Cas9 expression. FACS analysis performed at different time points showed no significant expression of Cas9 across the entire timeline of doxycycline treatment (14 days). Therefore we obtained frozen sample of another APTK organoid line expressing inducible Cas9 (pCW-Cas9 vector) and *AGK*/*NMT* sgRNAs (lenti-sgRNA-Puro vector) generated by Dr. Marina Pesic in the lab. These organoids were subjected to doxycycline treatment for 2-3 days and AGK knockout efficiency was determined in treated vs untreated (with Doxycycline) organoid samples. Doxycycline induction of Cas9 showed no significant difference between treated and untreated groups for both *AGK* and *NMT* lines when relative *AGK* mRNA levels were used as a readout (Figure 6B). However, to our

surprise, there was a small but significant difference in relative mRNA levels of *AGK* in samples without doxycycline induction when compared to control (NMT lines) as depicted in Figure 6A. This suggested a possibility of a leaky promoter. Doxycycline inducible promoters are frequently used in biology research however, expression of genes without the presence of an inducer is frequently reported in the literature(Pham *et al.*, 2008). This was in concordance with what we observed and therefore it most likely alluded to the presence of a leaky promoter. We had also confirmed the functionality of the doxycycline sample and knew for sure that it was working. Thus due to the presence of a strong possibility of a leaky promoter, we chose to discontinue working with pCW-Cas9 vector and with the idea of controlling Cas9 expression via inducible promoters. Thus, we chose to work with the SCAR vector. We cloned the appropriate sgRNA oligos into the SCAR-sgRNA-hygro vector and validated with sequencing. Based on the previous observations by other members in the lab, we chose to improve upon the transfection efficiencies of the SCAR vector. It is well known that the efficiency of transfection varies with reagent used and with the size of the vector plasmid to be transfected. Coupled with the fact that SCAR-Cas9-Blast was a very big vector (13.3 kb) and data from FACS analysis suggested failure in transduction, it was imperative to improve upon transfection efficiencies for the SCAR vectors since transfection efficiencies reflect upon generation of sufficient viral titre. Upon finding that Lipofectamine showed the most promising results, we thought of improving upon concentration methods for lentiviral titres and found that concentration using vivaspin columns worked the best. Lentiviruses are very fragile and therefore harsh concentration techniques like centrifugation at a very high speeds, leads to significant loss of functional lentiviral titre. Since Vivaspin columns rely on filtration mechanism, it works the best for functional lentiviral titre concentration. Despite the aforementioned optimization, we failed in generating successfully transduced organoid/cell lines. Upon troubleshooting, we figured that the pMD2.G plasmid had undergone a possible recombination event, ultimately leading to failure in generation of functional lentiviruses. Viral vectors are highly prone to recombination. Recombination usually occurs at the Long terminal repeats and/or multiple poly A tails, which are inevitably present in the lentiviral vectors for gene expression. Upon recombination, usually, the lentiviral vector resolves into two (or more) plasmids, one of which carries the

bacterial antibiotic resistance gene, and other, the transgene of interest. As a result, upon repeated transformation events (for maxi preps), only the plasmid harbouring the antibiotic resistance gene propagates. In order to test this we ran a simple gel with uncut plasmids and plasmids linearised with a single restriction enzyme (having a single site in the construct). When an uncut plasmid is run on a gel, 3 bands, two faint and one bright are to be expected. These 3 bands reflect the presence of three different structures of the plasmid in the sample, that are linear, nicked and supercoiled. Nicked or relaxed plasmid travel the slowest and the plasmids with supercoiled structure travel the fastest, amongst these three aforementioned structures. The supercoiled plasmid is the functional one and therefore should be visible as the brightest band on the gel, when compared to the other two. When the plasmid is linearised with a single restriction enzyme with a single site in the construct, a single bright band should be visible.

Upon running the gel for pMD2.G, we found that the site for NotI in our plasmid sample is probably absent, given the fact that digestion with NotI generated the exact same band pattern as the uncut one. According the vector map (Figure 15), the NotI site is present close to the □-globin poly A tail of the VSVG gene, and according to the gel data, SapI and AgeI show presence of multiple sites as reflected by multiple bands upon digestion. These facts further favour the hypothesis of recombination of pMD2.G at the poly A tail. Figure 8.C shows the difference between a recombined (Left) and “normal” or one that hasn’t undergone any recombination (right) pMD2.G plasmid. The sample in Figure 8.C right panel was maxi preped 4 years ago, and even in that sample one sees a very faint small size band in the SapI column indicating presence of some recombinant plasmids in the sample. Upon this finding of a possible faulty pMD2.G and usage of the correct MD2.G plasmid, we were successful in generating genetically modified organoid and cell lines. Since this was troubleshoot data we chose not to validate the recombination event, however the fact that the transductions worked after using the correct plasmids (which were verified by running a gel), provided substantial proof that the pMD2.G plasmid we were using was indeed faulty.

Figure 16: Vector map of pMD2.G.

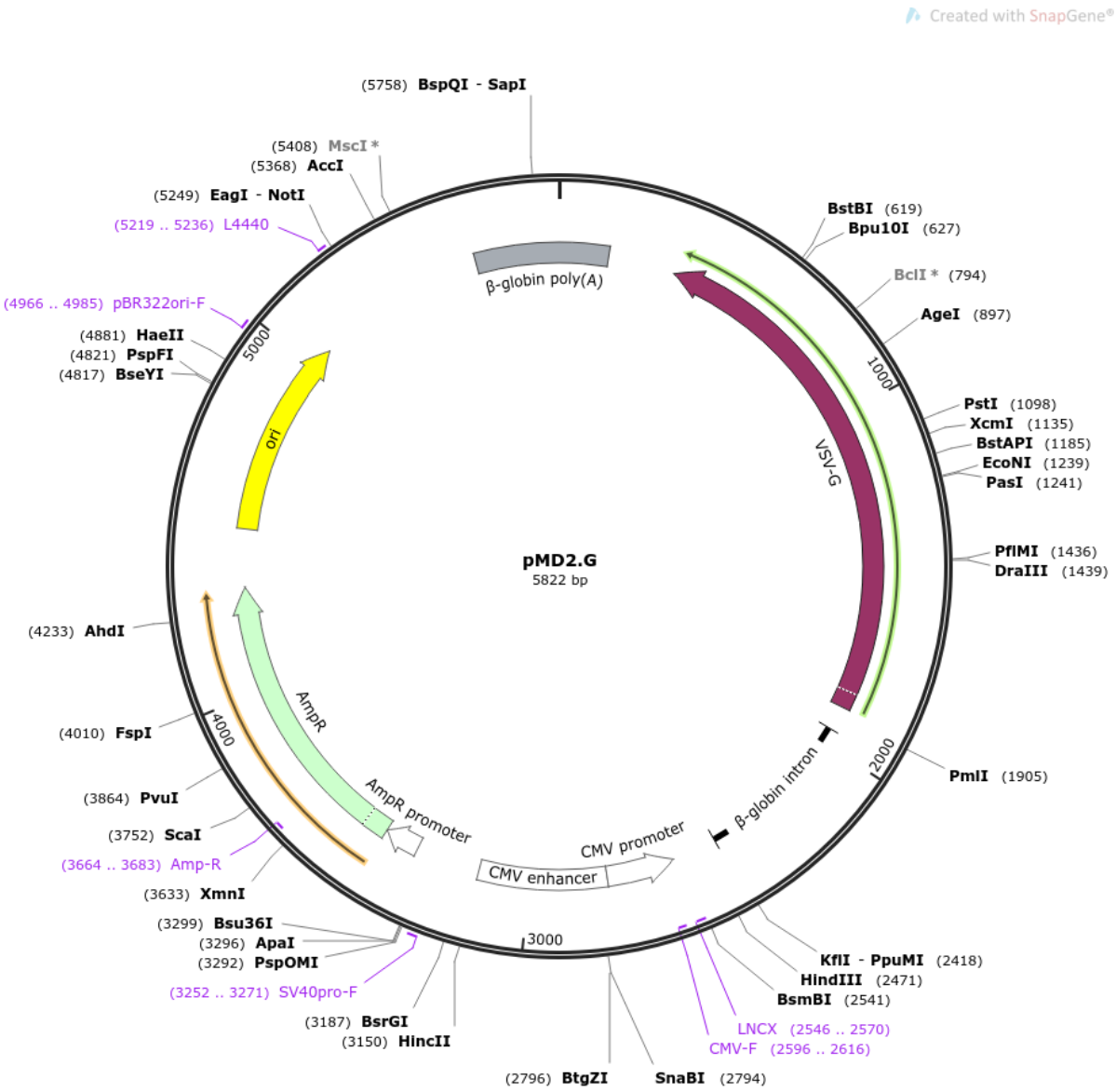

Description: Vector map of pMD2.G showing sites with loci for restriction enzymes. Notice the location of restriction sites for NotI, SapI and AgeI around the poly A tail. The generated data indicates recombination nearby and/or in the VSVG coding gene segment.

Figure source: Addgene

SCAR-Cas9 expressing APTK and CMT-93 cell lines were generated and when visualised for GFP expression showed faint-intermediate signal strength in case of both cell and organoid lines. This might be possible due to many reasons. For instance, according to an observation that the GFP signal intensity increases dramatically on the immediate next day after passaging and reduces as the organoids/cell lines grow, implied the confluency of the cell/organoid line reflects upon the intensity of GFP signal. This might be because of the increased growth and expression of proteins (including GFP) post-passaging. Another reason for variation in GFP intensity in individual organoids/cells could be because of the random integration of the transgene in the genome of organoids/cells. Lentiviral integration of the gene of interest during transductions is not specific, however occurs preferentially in the coding regions. Therefore it might be possible that some organoids/cells may express more GFP compared to others either due to the integration of transgenes downstream of strong promoters/enhancers or because of the occurrence of multiple integration events due to infection with more than one lentiviruses. In case of CMT-93, the intensity seems low most likely due to the extreme flat appearance of the cell line. However this may or may not necessarily correlate with the expression levels of Cas9. In the pSCAR-Cas9-blast vector the blasticidin resistance gene is linked to the Cas9 to ensure that the selection is specific to Cas9 expressing cells. The relative Cas9 mRNA levels as opposed to both control cell and organoids showed significant difference in a positive direction when quantified (Figure 11A & 13A).

APTK_Cas9 organoids were transduced with AGKsgRNAs expressing vectors (sgRNA #1 - #4). These organoids as opposed to *NMT* control showed significant difference in terms of rate of growth. The *AGK* knockout organoids showed a very slow growth rate as opposed to *NMT* control. This made sense given the fact that *AGK* is a kinase and kinases are heavily implicated in growth related pathways. Moreover, loss of AGK perturbs mitochondria function severely since it is involved in maintaining the structural integrity of the membrane as well as translocation of mitochondrial protein . However in order to validate the presence of a knockout, the organoids needed to be confluent enough for harvesting RNA for qPCR. Moreover the longer waiting duration may result in expansion of antibiotic resistant organoid

colonies. This may be one of the reasons why our quantification of AGK knockout didn't show a robust knockout on a qPCR plot. Because with time the antibiotic resistant and “Not knocked out” population of organoids proliferate, which may explain our results given the fact that we had to wait ~ one month for them to grow. Given the fact that the Cas9 was linked with the blasticidin resistant protein could also negatively impact the efficiency of CRISPR-Cas9 cleavage. However this seems unlikely as it’s known to work in other systems as reported in literature. Another possible reason for an inefficient knockout could be that the AGK sgRNA was inefficacious. The data shown above was for *AGK* sgRNA #3 expressing organoids. Organoids expressing the other guides were not growing enough to be quantified which may be because of a successful knockout. The efficacy of CRSIPR-Cas9 cleavage and knockout depends on the guide oligos and therefore since APTK organoids with AGKsgRNA #2 showed least growth, those might be harbouring a successful knockout for AGK.

All these hypothesis coupled with the observation that some stably transduced AGK sgRNA and Cas9 expressing organoids (Validated by confocal imaging of GFP and BFP) grow and some do not and some grow at an extremely slow rate compared to NMT control, supports the hypothesis that successful knockout of AGK perturbs growth of APTK organoids significantly, as the ones that grow do not show presence of a knockout. In order to find more theoretical evidence in favour/against of this hypothesis, we used APC, TGFBR2, TP53, KRAS and AGK as a gene query for genemania application in cytoscape. This revealed key interactions of AGK as reported in the literature as shown in figure 16. Out of the many possible ways in which AGK knockout might lead to stunted growth, its interaction with CSNK2A1 or casein kinase 2 alpha 1 seemed to be of interest. CSNK2A1 is a serine/threonine kinase involved in phosphorylation of acidic proteins like casein. It regulates various cellular processes like cell cycle control, apoptosis, and circadian rhythm. Pathways involving CSNK2A1 as one of the key players as revealed by the network generated in cytoscape include regulation of cellular protein catabolic processes, cell growth, signal transduction by p53 class mediator, etc, along with the ones mentioned before. In context of APTK organoids which essentially model human colorectal cancer, Wnt signalling pathways is one of the key pathways hyperactivated due to

deletion mutations in *APC*. CSNK2A1 is known to promote activation of Wnt signalling. Wang. et al in their paper find that in KRAS(G12C) mutant lung cancer cells, CSNK2A1 knockdown decreases cell proliferation, blocks Wnt/-catenin signalling, and intensifies the anti-proliferative effect of MEK inhibition(Wang *et al.*, 2019). According to Figure 16, AGK colocalizes and is coexpressed with CSNK2A1. Therefore it might be possible that AGK colocalization and coexpression is essential for CSNK2A1 function and its knockout renders CSNK2A1 non-functional leading to inhibition of Wnt signalling and therefore stunted growth and proliferation in APTK organoids, where hyperactive Wnt signalling is mandatory. Furthermore, AGK is also coexpressed and colocalised with PDE6D whose inhibition is known to inhibit KRAS signalling. Along with these AGK is also known to promote PI3K-Akt signalling pathway via PTEN inhibition, and interacts with JAK2 for STAT3 phosphorylation. Both of the aforementioned are heavily implicated in cell growth and differentiation and therefore AGK knockout may lead to stunted growth via perturbations in these pathways as well. AGK is also strongly co-expressed with FKBP1A which promotes apoptosis and is shown to negatively regulate glioblastoma growth(Cai *et al.*, 2022). Recent literature suggests that both FKBP1A and CSNK2A1 along with AGK are heavily implicated across cancers.

Figure 17: Gene interaction network of AGK with APC, TGFBR2, TP53 and KRAS.

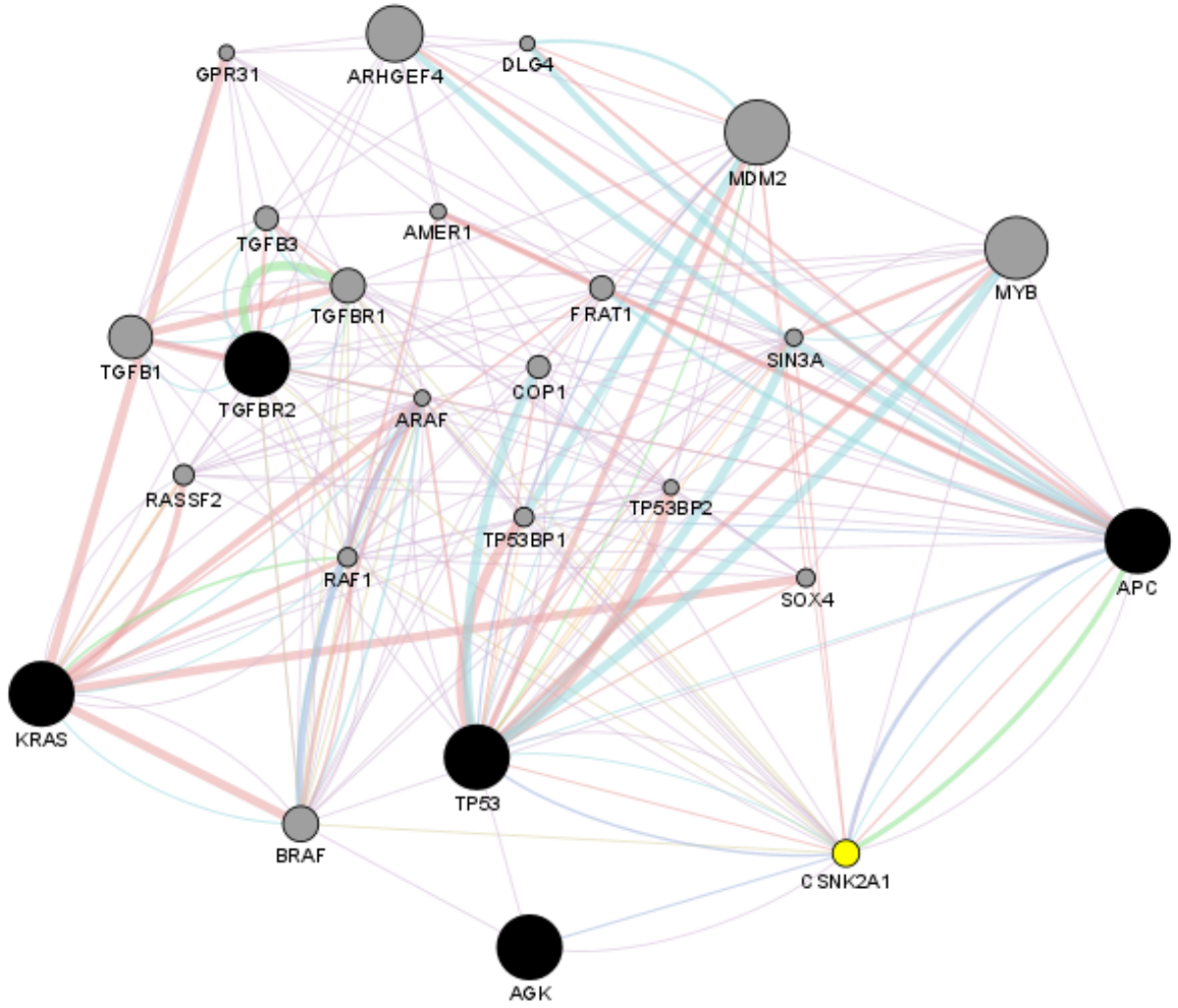

Description: Network interactions of AGK with the query genes along with key nodes (genes) obtained from the literature, relevant for this query are depicted with their respective interactions. Interactions are defined as Physical interactions, Co-expression, Co-localizations, genetic interactions, pathways, shared protein domains, and predicted interactions. Black nodes are the query nodes and grey nodes are the nodes obtained from literature. CSNK2A1 is highlighted in yellow and is known to interact with key players implicated in cancers like BRAF, TP53, APC, MDM2, TGFBR, etc. AGK is co-expressed with BRAF, TP53 and CSNK2A1 along with colocalization with CSNK2A1. Colors of the edges represent the type of network interactions. Red; physical interaction, purple; Co-expression, blue; Co-expression,

Green; genetic interactions, Cyan; Pathway interactions, Ochre; Predicted, grey; Shared protein domains.

For the validation of the SCAR vector system, we chose to generate a PDL1 knocked out line, and aimed to transplant the gene edited population post IDLV-cre infection in mice subcutaneously. If the SCAR vector system is efficacious then it would show increased T cell infiltration in PDL1 knockout tumors as opposed to control in the histological sections. In case of PDL1 knockout line generation, based on previous data in the lab which showed promising results, we opted to employ usage of only PDL1 sgRNA#4. When the polyclonal population was quantified we did see a difference in relative PDL1 mRNA levels but not a significant difference. This might be because of multiple reasons. For instance, insufficient Cas9 expression, lack of sgRNA efficacy for CRISPR-Cas9 cleavage, clonal variation in knockouts, etc. Therefore we opted to generate lines for all the PDl1 sgRNAs and perform limiting dilutions. When monoclonal populations of CMT-93-SCAR_Cas9-SCAR_PDL1sgRNA#4 were quantified for PDL1 expression, they showed difference in relative expression of PDL1 mRNA with clone #3 showing the least expression (Figure 14). Differential expression of Cas9 along with sgRNA efficiency might be one of the reasons for variation in knockout in a polyclonal population. Thus performing limiting dilutions is imperative for downstream analysis in order to have a uniform knockout. However it should also be taken into account that PDL1 expression varies from cell type to cell type and in case of CMT-93 the expression levels at basal state seem to be low, as observed from the mean Ct values in WT cell line which were around 30. Therefore it may not be completely appropriate to validate the knockout efficiency for PDL1 in vitro, where there is no selective pressure on the tumor cells to upregulate PDL1 expression as is observed in case of almost all tumors in natural systems. Moreover, it is imperative to quantify a knockout on protein level with either western blots, FACS, etc which could not be done in this thesis due to time constraints. Quantifications for knockout with a qPCR should not be a “gold standard” since mutated genes post to CRSIPR-Cas9 gene editing can still be transcribed and , if not cleared by the cellular machinery, will be

detected by qPCR primers, and therefore can give a false readout of a knockout on a qPCR plot. Usually, the mutated mRNAs are cleared by the nonsense mediated decay mechanism of the cell and therefore show lower mRNA copies compared to control on a qPCR plot. However, since the nonsense mediated decay mechanism only detects presence of premature stop codons, any other mutated mRNA transcribed from mutated gene, will be detected by the qPCR primers. Therefore quantification of knockout on protein level is imperative since mutated mRNAs should not generate functional proteins and misfolded proteins are cleared by the ubiquitin-proteasome degradation machinery.

Future experiments regarding the validation of AGK should include knockdown instead of knockout to observe its effects, taking into account the observation that *AGK* knockout blocks the growth of organoids *in vitro*. This can be done by usage of inhibitors, shRNAs, etc. Organoids should be subjected to limiting dilutions post genetic modifications in case of stable transductions in order to reduce variations in expression of proteins like Cas9 and should be checked regularly for non transduced antibiotic resistant colonies. In order to avoid this, samples can be maintained at a low concentrations and should be expanded only when required for experiments. For validation of the SCAR vector system via transplantation of PDL1 knocked out population post IDLV-Cre infection in mice, a model system expressing PDL1 at a higher levels compared to CMT-93 should be employed and knockouts need to be validated with western blots for protein level quantification. In depth understanding of the AGK function depending on cell type is imperative for drawing conclusions regarding its therapeutic potential. For instance, loss of AGK in CD8+ T cells reduces their anti-tumor activity. Kinases are heavily implicated in cancers including colorectal cancers, therefore a new kinome screen with the SCAR vector in CMT-93 line and its subsequent subcutaneous transplantation is an important future outlook. Recently whole genome screens are also performed and therefore can be done so in case of CRC as well with the usage of SCAR vector. This may reveal novel targets and may be easier to validate with the existing approach if not involved in growth directly. Given the fact that there are no specific/selective inhibitor for AGK because the functions of AGK in disease and pathology have not been fully elucidated, therefore designing novel inhibitors for AGK and treating the tumor *in vivo* seems to

have immense potential and value as a novel therapeutic target across cancers in conjuction with contemporary treatments. For this, in the future, to further understand the physiological and pathological functions of AGK, it will be required to further investigate its interaction networks and specific molecular targets.

References.

1. André, T et al. (2020). Pembrolizumab in Microsatellite-Instability-High Advanced Colorectal Cancer. N Engl J Med 383, 2207–2218.
2. Angell, H, and Galon, J (2013). From the immune contexture to the Immunoscore: the role of prognostic and predictive immune markers in cancer. Curr Opin Immunol 25, 261–267.
3. Baghban, R, Roshangar, L, Jahanban-Esfahlan, R, Seidi, K, Ebrahimi-Kalan, A, Jaymand, M, Kolahian, S, Javaheri, T, and Zare, P (2020). Tumor microenvironment complexity and therapeutic implications at a glance. Cell Commun Signal 18, 59.
4. Bektas, M, Payne, SG, Liu, H, Goparaju, S, Milstien, S, and Spiegel, S (2005). A novel acylglycerol kinase that produces lysophosphatidic acid modulates cross talk with EGFR in prostate cancer cells. J Cell Biol 169, 801–811.
5. Cai, S, Chen, Z, Tang, H, Meng, S, Tao, L, and Wang, Q (2022). Upregulated FKBP1A Suppresses Glioblastoma Cell Growth via Apoptosis Pathway. Int J Mol Sci 23, 14935.
6. Chu, B, Hong, Z, and Zheng, X (2021). Acylglycerol Kinase-Targeted Therapies in Oncology. Front Cell Dev Biol 9.
7. Dai, M, Yan, G, Wang, N, Daliah, G, Edick, AM, Poulet, S, Boudreault, J, Ali, S, Burgos, SA, and Lebrun, J-J (2021). In vivo genome-wide CRISPR screen reveals breast cancer vulnerabilities and synergistic mTOR/Hippo targeted combination therapy. Nat Commun 12, 3055.
8. Doench, JG et al. (2016). Optimized sgRNA design to maximize activity and minimize off-target effects of CRISPR-Cas9. Nat Biotechnol 34, 184–191.
9. Dubrot, J et al. (2021). In vivo screens using a selective CRISPR antigen removal lentiviral vector system reveal immune dependencies in renal cell carcinoma. Immunity 54, 571-585.e6.
10. Galluzzi, L, Senovilla, L, Vacchelli, E, Eggermont, A, Fridman, WH, Galon, J, Sautès-Fridman, C, Tartour, E, Zitvogel, L, and Kroemer, G (2012). Trial watch: Dendritic cell-based interventions for cancer therapy. Oncoimmunology 1, 1111–1134.

11. Galon, J et al. (2006). Type, Density, and Location of Immune Cells Within Human Colorectal Tumors Predict Clinical Outcome. Science 313, 1960–1964.
12. Galon, J, Angell, HK, Bedognetti, D, and Marincola, FM (2013). The continuum of cancer immunosurveillance: prognostic, predictive, and mechanistic signatures. Immunity 39, 11–26.
13. Galon, J, and Bruni, D (2019). Approaches to treat immune hot, altered and cold tumours with combination immunotherapies. Nat Rev Drug Discov 18, 197–218.
14. Galon, J, Fridman, W-H, and Pagès, F (2007). The adaptive immunologic microenvironment in colorectal cancer: a novel perspective. Cancer Res 67, 1883–1886.
15. Ganesh, K, Stadler, ZK, Cercek, A, Mendelsohn, RB, Shia, J, Segal, NH, and Diaz, LA (2019). Immunotherapy in colorectal cancer: rationale, challenges and potential. Nat Rev Gastroenterol Hepatol 16, 361–375.
16. Geraldo, LHM, Spohr, TCL de S, Amaral, RF do, Fonseca, ACC da, Garcia, C, Mendes, F de A, Freitas, C, dosSantos, MF, and Lima, FRS (2021). Role of lysophosphatidic acid and its receptors in health and disease: novel therapeutic strategies. Signal Transduct Target Ther 6, 45.
17. Guan, Y-F, Li, G-R, Wang, R-J, Yi, Y-T, Yang, L, Jiang, D, Zhang, X-P, and Peng, Y (2012). Application of next-generation sequencing in clinical oncology to advance personalized treatment of cancer. Chin J Cancer 31, 463.
18. Guinney, J et al. (2015). The consensus molecular subtypes of colorectal cancer. Nat Med 21, 1350–1356.
19. Hu, Z et al. (2019). Acylglycerol Kinase Maintains Metabolic State and Immune Responses of CD8+ T Cells. Cell Metab 30, 290-302.e5.
20. Kang, Y et al. (2017). Sengers Syndrome-Associated Mitochondrial Acylglycerol Kinase Is a Subunit of the Human TIM22 Protein Import Complex. Mol Cell 67, 457-470.e5.
21. M, J, K, C, I, F, M, H, Ja, D, and E, C (2012). A programmable dual-RNA-guided DNA endonuclease in adaptive bacterial immunity. Science 337.
22. Makhov, P, Sohn, JA, Serebriiskii, IG, Fazliyeva, R, Khazak, V, Boumber, Y,

Uzzo, RG, and Kolenko, VM (2020). CRISPR/Cas9 genome-wide loss-of-function screening identifies druggable cellular factors involved in sunitinib resistance in renal cell carcinoma. Br J Cancer 123, 1749–1756.

23. Mayr, JA et al. (2012). Lack of the mitochondrial protein acylglycerol kinase causes Sengers syndrome. Am J Hum Genet 90, 314–320.
24. Miller, KD, Nogueira, L, Mariotto, AB, Rowland, JH, Yabroff, KR, Alfano, CM, Jemal, A, Kramer, JL, and Siegel, RL (2019). Cancer treatment and survivorship statistics, 2019. CA Cancer J Clin 69, 363–385.
25. Mlecnik, B et al. (2011). Histopathologic-based prognostic factors of colorectal cancers are associated with the state of the local immune reaction. J Clin Oncol Off J Am Soc Clin Oncol 29, 610–618.
26. Pagès, F et al. (2009). In situ cytotoxic and memory T cells predict outcome in patients with early-stage colorectal cancer. J Clin Oncol Off J Am Soc Clin Oncol 27, 5944–5951.
27. Pham, DH, Moretti, PAB, Goodall, GJ, and Pitson, SM (2008). Attenuation of leakiness in doxycycline-inducible expression via incorporation of 3′ AU-rich mRNA destabilizing elements. BioTechniques 45, 155–162.
28. Pirona, AC, Oktriani, R, Boettcher, M, and Hoheisel, JD (2020). Process for an efficient lentiviral cell transduction. Biol Methods Protoc 5, bpaa005.
29. Plundrich, D, Chikhladze, S, Fichtner-Feigl, S, Feuerstein, R, and Briquez, PS (2022). Molecular Mechanisms of Tumor Immunomodulation in the Microenvironment of Colorectal Cancer. Int J Mol Sci 23, 2782.
30. Qiao, Y, Li, T, Zheng, S, and Wang, H (2018). The Hippo pathway as a drug target in gastric cancer. Cancer Lett 420, 14–25.
31. Ran, FA, Hsu, PD, Wright, J, Agarwala, V, Scott, DA, and Zhang, F (2013). Genome engineering using the CRISPR-Cas9 system. Nat Protoc 8, 2281–2308.
32. Ribas, A, and Wolchok, JD (2018). Cancer Immunotherapy Using Checkpoint Blockade. Science 359, 1350–1355.
33. Sanjana, NE, Shalem, O, and Zhang, F (2014). Improved vectors and genome-wide libraries for CRISPR screening. Nat Methods 11, 783–784.
34. Schmitt, M, and Greten, FR (2021). The inflammatory pathogenesis of colorectal cancer. Nat Rev Immunol 21, 653–667.

35. Shen, L et al. (2007). Integrated genetic and epigenetic analysis identifies three different subclasses of colon cancer. Proc Natl Acad Sci U S A 104, 18654–18659.
36. Son, H-Y, and Jeong, H-K (2021). Immune Evasion Mechanism and AXL. Front Oncol 11.
37. Traxler, P (2003). Tyrosine kinases as targets in cancer therapy - successes and failures. Expert Opin Ther Targets 7, 215–234.
38. Varanasi, SK, Kumar, SV, and Rouse, BT (2020). Determinants of Tissue-Specific Metabolic Adaptation of T Cells. Cell Metab 32, 908–919.
39. Varga, J et al. (2020). AKT-dependent NOTCH3 activation drives tumor progression in a model of mesenchymal colorectal cancer. J Exp Med 217, e20191515.
40. Wang, H, Lv, Q, Xu, Y, Cai, Z, Zheng, J, Cheng, X, Dai, Y, Jänne, PA, Ambrogio, C, and Köhler, J (2019). An integrative pharmacogenomics analysis identifies therapeutic targets in KRAS-mutant lung cancer. EBioMedicine 49, 106–117.
41. Yang, H, Wang, Y, Wang, P, Zhang, N, and Wang, P (2022). Tumor organoids for cancer research and personalized medicine. Cancer Biol Med 19, 319–332.